ARTICLE IN PRESS

ISA Transactions xxx (xxxx) xxx



Contents lists available at ScienceDirect

ISA Transactions

journal homepage: www.elsevier.com/locate/isatrans



Practice article

Design and experimental evaluation of block-pulse functions and Legendre polynomials observer for attitude-heading reference system

Jafar Keighobadi^a, Javad Faraji^{a,*}, Farrokh Janabi-Sharifi^b, Mohammad Ali Hamed^a

- ^a Faculty of Mechanical Engineering, University of Tabriz, Tabriz, Iran
- ^b Department of Mechanical and Industrial Engineering, Ryerson University, Toronto, ON, Canada

ARTICLE INFO

Article history: Received 22 June 2020 Received in revised form 12 January 2021 Accepted 12 January 2021 Available online xxxx

Keywords:
Orthogonal hybrid functions
Legendre polynomials
Block-pulse functions
Duality
AHRS
MEMS

ABSTRACT

The main purpose of this paper is design and implementation of a new linear observer for an attitude and heading reference system (AHRS), which includes three-axis accelerometers, gyroscopes, and magnetometers in the presence of sensors and modeling uncertainties. Since the increase of errors over time is the main difficulty of low-cost micro electro mechanical systems (MEMS) sensors producing instable on-off bias, scale factor (SF), nonlinearity and random walk errors, development of a high-precision observer to improve the accuracy of MEMS-based navigation systems is considered. First, the duality between controller and estimator in a linear system is presented as the base of design method. Next, Legendre polynomials together with block-pulse functions are applied for the solution of a common linear time-varying control problem. Through the duality theory, the obtained control solution results in the block-pulse functions and Legendre polynomials observer (BPLPO). According to product properties of the hybrid functions in addition to the operational matrices of integration, the optimal control problem is simplified to some algebraic equations which particularly fit with low-cost implementations. The improved performance of the MEMS AHRS owing to implementation of BPLPO has been assessed through vehicle field tests in urban area compared with the extended Kalman filter (EKF).

© 2021 ISA. Published by Elsevier Ltd. All rights reserved.

1. Introduction

Motivation. Obtaining accurate orientation information in autonomous vehicles and robotic systems has recently attracted valuable efforts of navigation researchers and engineers. The AHRS is equipped with an inertial measurement unit (IMU) including 3-axis gyroscopes and accelerometers as well as auxiliary magnetometers, odometer, and GPS in communication with a computational unit. Therefore, the measured data of all sensors are integrated in state estimation filters to optimally compute the attitude and heading angles data of carrying vehicle. Large value uncertainties of low-cost sensors in particular instable biases, random walk noise and nonlinearities may lead to considerable imperfections in orientation, velocity, and position vector of the navigation systems, which make the MEMS sensors unreliable [1]. Hence, the development of proper estimation filters/observers for the integration of MEMS grade sensors data should be exploited in the low-cost AHRS with optimal performance.

E-mail addresses: keighobadi@tabrizu.ac.ir (J. Keighobadi), j.faraji@tabrizu.ac.ir (J. Faraji).

https://doi.org/10.1016/j.isatra.2021.01.027

0019-0578/© 2021 ISA. Published by Elsevier Ltd. All rights reserved.

Related literature. The minimal representation of orientation by Euler angles was commonly applied either in KF [2], or its extended shape EKF [3,4]. Merhav and Koifman have implemented the EKF method to real-time estimation in a remotely piloted vehicle, with assuming that gyroscopes, magnetometers, wind speed, and barometer sensors produce raw data [5]. Orientation angles estimation by removal of gyroscopes and based on uncalibrated magnetometers data was proposed by Crassidis and Markley. The newly developed predictive filtering algorithm requires complicated computations owing to applying an unscented approximation method [6], compared with the EKF [7]. Based on KF, Zhu et al. introduced new state components for attitude and heading angles according to gravity and magnetic field of earth along the body axes of a vehicle [8]. Batista et al. presented a cascade observer of the AHRS together with the asymptotic stability analysis. Though the magnetometers were affected by hard- and soft-iron perturbations, the calibration of TAM has not been carried out [9]. By use of the inertial sensors, GPS data, and uncalibrated magnetometers, Martin and Salaün developed an invariant observer to estimate the orientation components by AHRS and showed the main advantage of low computational burden with respect to EKF [10]. Sabatini utilized an EKF to determine the AHR angles by use of inertial and magnetic sensors, so that the noise covariance matrices of the accelerometers and

^{*} Corresponding author at: Faculty of Mechanical Engineering, University of Tabriz, Tabriz, 51666-16444, Iran.

Nomenclature	
a, b, c, d, e	Three-axis magnetometers (TAM)
	calibration coefficients
\mathbf{a}_{C}	Coriolis acceleration vector
\mathbf{a}_{d}	Dynamic acceleration vector
b_{nm}	Hybrid function element
C_n^b	Navigation frame to body frame
	transfer matrix
$\mathbf{f}(\mathbf{x}, \mathbf{u})$	Nonlinear dynamics vector
$\begin{bmatrix} f_x^b & f_y^b & f_z^b \end{bmatrix}^T$	Accelerometers measure along
	body axes
$\boldsymbol{F}_i, \boldsymbol{G}_i, \boldsymbol{H}_i, \boldsymbol{D}_i$	Discrete system matrices
g	Gravitational acceleration
$\mathbf{g}^b = \begin{bmatrix} \mathbf{g}_x^b & \mathbf{g}_y^b & \mathbf{g}_z^b \end{bmatrix}^T$	Gravitational acceleration vector
h(x)	Nonlinear measurement vector
I	Identity matrix
J	Cost function
$m=0\ldots M-1$	Order of Legendre polynomials
$\begin{bmatrix} M_x^b & M_y^b & M_z^b \end{bmatrix}^T$	Measured magnetic field vector
$n=1\ldots N$	Order of block-pulse functions
N, E, D	North, East, Down Axes
N_T	Number of test data for calibra-
	tion
$P_{m}\left(t\right)$	Legendre polynomials
\mathbf{Q}, \mathbf{R}	Covariance matrices of process,
.	measurement noises
R_{zy}	Gramian matrix for vectors z and
.	y set
t	Normalized time
t_f	Final time
$\boldsymbol{u}, \boldsymbol{y}$	Input and output in the deterministic model
v	Measurement noise vector
$\mathbf{w} = \begin{bmatrix} w_{x} & w_{y} & w_{z} \end{bmatrix}^{T}$	
[xyz]	vector
X	AHRS state vector
X_i, Y_i, Z_i	Inertial frame components
X_b, Y_b, Z_b	Body frame components
X_e, Y_e, Z_e	Earth frame components
Â	Estimate of x
z , y	Input and output vectors in
	stochastic model
\mathbf{z}^d	Dual basis for z
$\hat{f z}_{ f y}$	Projection of \mathbf{z} on \mathcal{L} { \mathbf{y} }
$\alpha \in S$	Element α of set S
λ	Lagrange multiplier
φ, θ, ψ	Roll, Pitch, Heading
ψ_m	Calibrated heading angle
ψ_{GPS}	Heading angle obtained from GPS
ψ_{raw}	Raw heading angle of TAM
ω_e	Earth rotation rate
$oldsymbol{\omega}_{ib}^{b}$	Rotation rate measured by gyro-
ω ⁿ	scopes Rotation rate of earth
ω_{ie}^n	Rotation rate of N, E, D frame
$\boldsymbol{\omega}_{en}^n$	
$\begin{bmatrix} \omega_{x} & \omega_{y} & \omega_{z} \end{bmatrix}^{T}$	Measured angular velocity vector
Γ s ₂₀₁ s ₂₀₁ s ₂₀₁ Τ	by gyroscopes
$\begin{bmatrix} \delta w_x & \delta w_y & \delta w_z \end{bmatrix}^T$	Gyroscopes bias vector
$col\{a,b\}$	Column vector of a and b

$diag\{a,b\}$	Diagonal matrix of a and b
$\langle \mathbf{z}_i,\mathbf{z}_j angle$	Inner product of two column vectors \mathbf{z}_i and \mathbf{z}_i
$\{\mathbf{z}_i\}$	Set of vectors \mathbf{z}_i
$\mathcal{L}\left\{\mathbf{z},\mathbf{y}\right\}$	A linear span of variables $\{z, y\}$
$\ \boldsymbol{x}\ ^2$	Squared norm 2 of vector x
\otimes	Kronecker product
.d	Dual basis
. T	Matrix transpose
•*	Complex conjugation; Hermitian trans-
	position
\mathbb{R}^n	n-dimensional real space

magnetometers are determined adaptively [11]. Considering the acceleration measured by external accelerometers and gravity vector components in the body frame, Lee et al. estimated attitude angles in accelerated motions with KF [12]. By use of gravity and the earth's magnetic fields as two measured values. Martin and Salaün proposed a new attitude estimation [13]. With considering gyroscopes, accelerometers, magnetometers, and true air-speed sensors, Ali et al. proposed a new method for estimating the attitude to minimize the growth of error in the combined data in auxiliary gyroscopes [14]. Markley provided a comparison of the attitude by use of two measurement vectors, and showed that the heading angle could be obtained using magnetometers and accelerometers data [15]. Rehbinder and Hu provided a new solution to drift free attitude estimation of robotic applications with integration of IMU-based sensors' data and showed that adaptive filters and accurate selection of parameters could be significant when examining various movements, including the phases of deceleration and high acceleration [16]. Tang et al. presented a novel square-root cubature KF (CKF) algorithm for attitude estimation purpose; in which the dynamic model involves gyroscopes data with quaternion description [17]. Huang et al. investigated the integration of low-cost GPS sensors' data on the vehicle for the AHRS by use of the CKF [18]. Development of a novel algorithm without exploiting gyroscopes data should result in a decrease of sensors cost as well as orientation angles errors in the AHRS. This method of De Celis and Cadarso requires the combination of multi-sensor data, which is unsuitable for complex practical systems [19]. Soken and Hajiyev's gain-correction via robust unscented KF (UKF) for picosatellite attitude estimation was based on the faults mode of measurement vector [20]. Blondy et al. introduced a novel KF algorithm of interacting multiple models for integration of star-tracker and gyroscopes sensors [21]. A robust attitude observer is applicable on a combination of GPS receivers, magnetometers, angular rate and gravity sensors in accelerated experimental environments as proposed by No et al. [22]. To synchronized removal of nonlinearity errors of Euler angles dynamics and magnetic field disturbances, multiplicated quaternions in an adaptive KF were applied by Zhang and Nie [23]. Yang et al. proposed a singular value decomposition of CKF with adaptive variable methods to estimate the orientation components by AHRS in a small unmanned aerial vehicle in complicated maneuvering conditions [24].

The defects of the related earlier methods are dividable into two groups. The first group of the KF and its derivatives like UKF and CKF solve the nonlinear estimation problem by linearizing state and/or measurement equations, and then applying the standard KF on the resulting linearized system. This linearization yields approximation errors which the filter does not take into account in the prediction/update step [2–5,7,8,11–24]. In these methods, the uncertainty is considered as a Gaussian white noise

which does not cover some major uncertainties of MEMS sensors in AHRS. Therefore, the EKF errors tend to underestimate model uncertainties; while the CKF and UKF methods impose a heavy computational burden. The second defect, which also may affect the uncertainty bound, is the leakage due to using uncalibrated sensors [6,9,10]. In most papers, the raw data of magnetometers are fed to the AHRS, while magnetometers data are affected by hard- and soft-iron anomalities [25,26]. Therefore, in the estimation algorithm of AHRS angles of the vehicle, high-precision approximation functions and observers should be considered.

In recent few years, as well-known hybrid functions, Legendre polynomials and the block-pulse functions have been used to solve nonlinear Volterra–Fredholm equations [27], optimal control of nonlinear systems [28], and integral-differential equation [29]. These functions resulted in a decrease of processing time, required memory and the effective change of differential equations to algebraic kind [30].

Contribution. In this paper, the main contribution is design of a new linear observer through duality theory and hybrid functions and its implementation in an AHRS for vehicular navigation purposes. The distinctive and new features of the proposed system are:

- A general observer system by use of hybrid functions is presented, which can be easily applied upon most physical systems.
- The hybrid functions of Legendre polynomials and blockpulse type have been considered to increase the accuracy, and also appropriate implementation in practice due to their linear property.
- A calibration algorithm on raw data of magnetometers is performed to increase the accuracy of AHRS.
- By use of available high-quality processors, the proposed method is satisfactorily applied in real-time. According to the data of INS/ GPS in urban area tests on a ground vehicle, the accuracy and computational efficiency of the newly proposed linear observer have been investigated.
- With considering duality theory, a new observer based on controller design of deterministic systems is presented where the uncertainties are modeled as a 2-norm upper bound signal rather than white Gaussian noise of KF. Unlike the white Gaussian noise, the energy-bounded disturbance model in the proposed deterministic observer involves different aspects of uncertainties of low-cost MEMS sensors.

Section 2 presents AHRS model and magnetometers calibration. In Section 3, duality theory, hybrid block-pulse and Legendre polynomials are represented. Through entering hybrid functions in linear control systems, design process, implementation and tests of the proposed BPLPO are presented in Section 4. Concluding are expressed in Section 5.

2. Mathematical description of strapdown AHRS

In this section, the modeling equations of the AHRS are described. Multiple Cartesian coordinates of inertial frame (X_i, Y_i, Z_i) , earth frame (X_e, Y_e, Z_e) , body frame (X_b, Y_b, Z_b) , and navigation frame along north, east, and down (N, E, D) directions are involved in the AHRS model as shown in Fig. 1 [31]. The inertial frame has non-rotating axes with respect to distant stars, and the earth frame axes rotate at earth's angular velocity (ω_e) with respect to the inertial frame.

According to Fig. 1, θ about Y_b -axis, φ about X_b -axis, and ψ about Z_b -axis constitute the orientation pitch, roll , and heading angles, respectively. From the navigation frame to body coordinate frame transformation matrix is obtainable as [32] given in Box I:

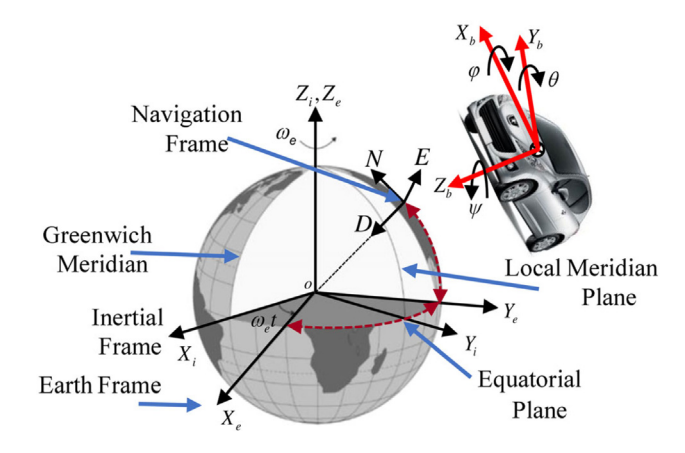


Fig. 1. Coordinate frame in using inertial navigation [26].

Based on components of the angular velocity in body frame as $\boldsymbol{\omega}_{nb}^b = \begin{bmatrix} \omega_x & \omega_y & \omega_z \end{bmatrix}^T$, the Euler angles dynamics is obtained as [33]:

$$\begin{cases} \dot{\varphi} = (\omega_{y} \sin \varphi + \omega_{z} \cos \varphi) \tan \theta + \omega_{x} \\ \dot{\theta} = (\omega_{y} \cos \varphi - \omega_{z} \sin \varphi) \\ \dot{\psi} = (\omega_{y} \sin \varphi + \omega_{z} \cos \varphi) \sec \theta \end{cases}$$
 (2)

$$\begin{bmatrix} \omega_{x} & \omega_{y} & \omega_{z} \end{bmatrix}^{T} = \boldsymbol{\omega}_{ib}^{b} - \boldsymbol{C}_{n}^{b}(\boldsymbol{\omega}_{ic}^{n} + \boldsymbol{\omega}_{en}^{n})$$
 (3)

where, the rotation rates of body frame with respect to inertial frame, $\boldsymbol{\omega}_{ib}^b$ are measured by strapdown gyroscopes along the body axes. $\boldsymbol{\omega}_{ie}^n$ and $\boldsymbol{\omega}_{en}^n$ stand for the rotation rates of earth frame and rotation rate of navigation frame with respect to inertial frame and earth frame, respectively. The superscript, for example n denotes that the vector projection is in the navigation n-frame. Due to very small amount of the earth's rotation velocity, ω_e , and very large curvature radius of the earth, $\mathbf{C}_n^b(\boldsymbol{\omega}_{ie}^n+\boldsymbol{\omega}_{en}^n)$ can be ignored and thus $\boldsymbol{\omega}_{ib}^b\approx\boldsymbol{\omega}_{nb}^b$ is obtainable. Along with the pure angular velocity $\boldsymbol{\omega}_{nb}^b$, the noises as $\mathbf{w}=\begin{bmatrix}w_x&w_y&w_z\end{bmatrix}^T$ and biases vector $\delta\mathbf{w}=\begin{bmatrix}\delta w_x&\delta w_y&\delta w_z\end{bmatrix}^T$ are considered on the gyroscopes outputs. Therefore, Eq. (2) leads to:

$$\begin{bmatrix} \dot{\varphi} \\ \dot{\theta} \\ \dot{\psi} \end{bmatrix} = \begin{bmatrix} 1 & \sin\varphi \tan\theta & \cos\varphi \tan\theta \\ 0 & \cos\varphi & -\sin\varphi \\ 0 & \sin\varphi \sec\theta & \cos\varphi \sec\theta \end{bmatrix} (\boldsymbol{\omega}_{nb}^{b} + \mathbf{w} + \delta\mathbf{w})$$
(4)

Eq. (4) can be rewritten as:

$$\dot{\mathbf{x}} = \mathbf{f}(\mathbf{x}, \mathbf{u}) + \mathbf{w}$$

$$= \begin{bmatrix}
(\omega_{x} + \delta w_{x}) + (\omega_{y} + \delta w_{y}) \sin \varphi \tan \theta + (\omega_{z} + \delta w_{z}) \cos \varphi \tan \theta \\
(\omega_{y} + \delta w_{y}) \cos \varphi - (\omega_{z} + \delta w_{z}) \sin \varphi \\
(\omega_{y} + \delta w_{y}) \sin \varphi \sec \theta + (\omega_{z} + \delta w_{z}) \cos \varphi \sec \theta
\end{bmatrix}$$

$$+ \mathbf{w} \tag{5}$$

The nonlinear vector $\mathbf{f}(\mathbf{x}, \mathbf{u})$ characterizing the AHRS dynamical system involves the state vector $\mathbf{x} = \begin{bmatrix} \varphi & \theta & \psi \end{bmatrix}^T$ and the input vector \mathbf{u} of the AHRS system by gyroscopes. By ignoring noise and uncertainty terms, Eq. (5) yields the orientation angles φ , θ , and ψ .

2.1. Output vector

Inertial accelerometers and non-inertial magnetometers are used to produce auxiliary outputs in the strapdown AHRS. Through 3-axis orthogonal gyroscopes, the angular rate of the vehicle is measured in the body frame. However, measurements

ISA Transactions xxx (xxxx) xxx

$$\mathbf{C}_{n}^{b} = \begin{bmatrix} \cos\theta\cos\psi & -\cos\varphi\sin\psi + \sin\varphi\sin\theta\cos\psi & \sin\varphi\sin\psi + \cos\varphi\sin\theta\cos\psi \\ \cos\theta\sin\psi & \cos\varphi\cos\psi + \sin\varphi\sin\theta\sin\psi & -\sin\varphi\cos\psi \\ -\sin\theta & \sin\varphi\cos\theta & \cos\varphi\cos\theta \end{bmatrix}$$
(1)

Box I.

of the gyroscopes in AHRS deteriorate over time due to integrating of uncertainties like stochastic noises, instable bias, SF and nonlinearities. Therefore, aiding data of accelerometers and magnetometers are considered in the measurement vector of observer. The accelerometers measure components of the earth gravity field of AHRS together with dynamic and Coriolis accelerations as:

$$\begin{bmatrix} f_x^b & f_y^b & f_z^b \end{bmatrix}^T = \mathbf{a}_d + \mathbf{a}_C + \mathbf{g}^b$$
 (6)

where $\mathbf{g}_{x}^{b}=-g\sin\theta$, $\mathbf{g}_{y}^{b}=g\cos\theta\sin\varphi$, and $\mathbf{g}_{z}^{b}=g\cos\theta\cos\varphi$ are projected gravity of the earth along body frame axes. Dynamic \mathbf{a}_{d} and Coriolis \mathbf{a}_{C} accelerations in Eq. (6) guide to error in the computation of roll and pitch by accelerometers of AHRS. Therefore, by taking into account the dynamic and Coriolis accelerations as disturbances, Eq. (6) is corrected as:

$$\begin{bmatrix} f_x^b & f_y^b & f_z^b \end{bmatrix}^T = \mathbf{g}^b + \mathbf{v} \tag{7}$$

where \mathbf{v} is modeled as a stochastic noise of the sensors and/or disturbances. While GPS data are available, the track angle of GPS can be used as the heading angle in on-ground applications. Accordingly, the measurement vector \mathbf{v} is completed as:

$$\mathbf{y} = \begin{bmatrix} f_x^b & f_y^b & f_z^b & \psi_{GPS} \end{bmatrix}^T = \mathbf{h} (\mathbf{x})$$

$$\mathbf{h} (\mathbf{x}) = \begin{bmatrix} -g \sin \theta & g \cos \theta \sin \varphi & g \cos \theta \cos \varphi & 1 \end{bmatrix}^T$$
(8)

where $\mathbf{h}(\mathbf{x})$ is a nonlinear vector characterizing the AHRS measurement vector. Aided navigation system with 3-axis magnetometers generates a new heading angle ψ_m , which can be replaced in Eq. (8) during outages of GPS signals as:

$$\mathbf{y} = \begin{bmatrix} f_x^b & f_y^b & f_z^b & \psi_m \end{bmatrix}^T \tag{9}$$

The above-mentioned noise of dynamic system Eq. (5) and measurement Eq. (7) as, \mathbf{w} and \mathbf{v} arise by instable parameters of sensors, local magnetic disturbances and non-gravitational accelerations.

2.2. Calibration of a three-axis magnetometers

The vector components of the earth magnetic field are measured using orthogonal TAM along the orthogonal axes of the body frame. However, hard- and soft-iron magnetic disturbances extremely impact on the accuracy of orientation angles by the AHRS [26]. Therefore, accurate navigation through magnetic sensors requires a calibration process. When the TAM system is in balance status, the φ and θ angles are zero. Hence, the heading angle $\psi_{\rm raw}$ is obtained as:

$$\psi_{\text{raw}} = -\tan^{-1}\left(\frac{M_y^h}{M_x^h}\right) \tag{10}$$

where M_x^h and M_y^h stand for measured the earth magnetic field components by TAM [26]. However, in unbalanced situation of TAM, the horizontal components M_x^h and M_y^h should be obtained through leveling of measurements by φ and θ angles:

$$\begin{bmatrix} M_{\chi}^{h} \\ M_{y}^{h} \end{bmatrix} \begin{bmatrix} \cos \theta & \sin \theta \sin \varphi & \cos \varphi \sin \theta \\ 0 & \cos \varphi & -\sin \varphi \end{bmatrix} \begin{bmatrix} M_{\chi}^{b} \\ M_{y}^{b} \\ M_{z}^{b} \end{bmatrix}$$
(11)

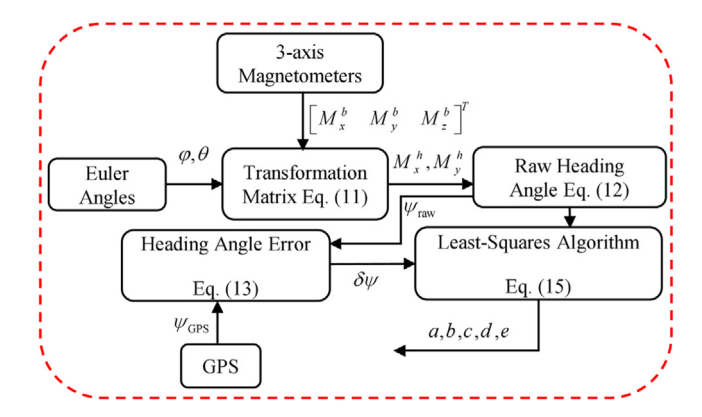


Fig. 2. Swinging calibration for a TAM.

where $\begin{bmatrix} M_x^b & M_y^b & M_z^b \end{bmatrix}^T$ shows the measured magnetic field. Now, considering the singular points of Eq. (10), the heading angle is obtained as:

$$\psi_{\text{raw}} = \begin{cases} 90 & M_{\chi}^{h} = 0, M_{y}^{h} < 0\\ 270 & M_{\chi}^{h} = 0, M_{y}^{h} > 0\\ 180 - \tan^{-1} \left(\frac{M_{y}^{h}}{M_{\chi}^{h}}\right) \times \frac{180}{\pi} & M_{\chi}^{h} < 0\\ -\tan^{-1} \left(\frac{M_{y}^{h}}{M_{\chi}^{h}}\right) \times \frac{180}{\pi} & M_{\chi}^{h} > 0, M_{y}^{h} < 0\\ 360 - \tan^{-1} \left(\frac{M_{y}^{h}}{M_{\chi}^{h}}\right) \times \frac{180}{\pi} & M_{\chi}^{h} > 0, M_{y}^{h} > 0 \end{cases}$$

$$(12)$$

In calibration of TAM based on swinging method of Fig. 2, ψ_{raw} is calibrated online through fitting on reference heading angle of GPS [26]. The heading angle error with respect to reference angle is computed by the swinging coefficients a through e as follows.

$$\delta\psi = \psi_{\text{GPS}} - \psi_{\text{raw}}$$

$$\delta\psi = a + b\sin(\psi_{\text{raw}}) + c\cos(\psi_{\text{raw}}) + d\sin(2\psi_{\text{raw}})$$

$$+ e\cos(2\psi_{\text{raw}})$$
(13)

Eq. (14) shows a truncated Fourier series of raw heading angle which is rearranged as a regression of calibration parameters given as in Box II. where N_T shows the number of test data for calibration of TAM. After obtaining coefficients a to e, the calibrated heading angle is obtained as:

$$\psi_m = a + b \sin(\psi_{\text{raw}}) + c \cos(\psi_{\text{raw}}) + d \sin(2\psi_{\text{raw}}) + e \cos(2\psi_{\text{raw}})$$
(16)

3. Control and estimation duality

Based on geometric and algebraic interpretation, random variables are considerable as vectors in certain linear spaces. According to the theory of dual basis, orthogonal complements, and duality principle of control and estimation in linear systems, the estimation algorithm is obtainable through linear control equations. Using the Gramian matrix and dual basis expressed in Appendix [26], Lemma 1 can be expressed [34].

$$\begin{bmatrix} \delta \psi_{1} \\ \delta \psi_{2} \\ \vdots \\ \delta \psi_{N_{T}} \end{bmatrix} = \begin{bmatrix} 1 & \sin(\psi_{\text{raw}_{1}}) & \cos(\psi_{\text{raw}_{1}}) & \sin(2\psi_{\text{raw}_{1}}) & \cos(2\psi_{\text{raw}_{1}}) \\ 1 & \sin(\psi_{\text{raw}_{2}}) & \cos(\psi_{\text{raw}_{2}}) & \sin(2\psi_{\text{raw}_{2}}) & \cos(2\psi_{\text{raw}_{2}}) \\ \vdots & \vdots & \vdots & \vdots & \vdots \\ 1 & \sin(\psi_{\text{raw}_{N_{T}}}) & \cos(\psi_{\text{raw}_{N_{T}}}) & \sin(2\psi_{\text{raw}_{N_{T}}}) & \cos(2\psi_{\text{raw}_{N_{T}}}) \end{bmatrix} \begin{bmatrix} a \\ b \\ c \\ d \\ e \end{bmatrix}$$

$$(15)$$

Box II.

Lemma 1 (Dual of Calculated Projections). The projection of \mathbf{z} on $\mathcal{L}\{\mathbf{y}\}$ can be calculated as $\hat{\mathbf{z}}_{|\mathbf{y}} = -\mathbf{R}_{z^d}^{-1}\mathbf{R}_{z^dy^d}\mathbf{y}$, in which $\{\mathbf{R}_{z^d}, \mathbf{R}_{z^dy^d}\}$ are the Gramian matrix of dual basis of vectors $\{\mathbf{z}^d, \mathbf{y}^d\}$ obtained as follows:

$$\begin{aligned}
\mathbf{R}_{z^d}^{-1} \mathbf{R}_{z^d y^d} &= -\mathbf{R}_{zy} \mathbf{R}_y^{-1} \\
\|\tilde{\mathbf{z}}_{|y}\|^2 &= \mathbf{R}_{\bar{z}} \\
\langle \tilde{\mathbf{z}}_{|y}, \tilde{\mathbf{z}}_{|y} \rangle &= (\mathbf{R}_z^{-1} + \mathbf{H}^* \mathbf{R}_v^{-1} \mathbf{H})^{-1}
\end{aligned} \tag{17}$$

The linear measurement model of Eq. (9) is expressed as:

$$\mathbf{y} = \mathbf{H}\mathbf{z} + \mathbf{v} = \begin{bmatrix} \mathbf{H} & \mathbf{I} \end{bmatrix} \begin{bmatrix} \mathbf{z} \\ \mathbf{v} \end{bmatrix}$$
 (18)

Therefore, the Gramian matrices of ${\bf z}$ and ${\bf v}$ are computable as:

$$\left\langle \begin{bmatrix} \mathbf{z} \\ \mathbf{v} \end{bmatrix}, \begin{bmatrix} \mathbf{z} \\ \mathbf{v} \end{bmatrix} \right\rangle = \begin{bmatrix} \mathbf{R}_{z} & 0 \\ 0 & \mathbf{R}_{v} \end{bmatrix}$$

$$\det \mathbf{R}_{z} \neq 0$$

$$\det \mathbf{R}_{v} \neq 0$$
(19)

Also, using the Gramian matrix and dual basis expressed in Appendix, Lemma 2 for linear models and dual basis can be expressed [34].

Lemma 2 (*Linear Models and Dual Basis*). Suppose $\{\mathbf{z}, \mathbf{y}\}$ satisfy $\mathbf{y} = \mathbf{Hz} + \mathbf{v}$, then the dual basis $\{\mathbf{z}^d, \mathbf{y}^d\}$ will satisfy the following linear model [34]:

$$\mathbf{z}^d = -\mathbf{H}^* \mathbf{v}^d + \mathbf{v}^d \tag{20}$$

where $\mathbf{y}^d = \mathbf{R}_v^{-1} \mathbf{v}$, $\mathbf{v}^d = \mathbf{R}_z^{-1} \mathbf{z}$. We also have the identities

$$R_{zy}R_y^{-1} = R_zH^* (R_v + HR_zH^*)^{-1} = (R_z^{-1} + H^*R_v^{-1}H)^{-1}H^*R_v^{-1}$$

= $-R_{zd}^{-1}R_{zdvd}$

and $\langle \tilde{\mathbf{z}}_{|\mathbf{y}}, \tilde{\mathbf{z}}_{|\mathbf{y}} \rangle = \mathbf{R}_{\tilde{\mathbf{z}}} = (\mathbf{R}_{\mathbf{z}}^{-1} + \mathbf{H}^* \mathbf{R}_{\mathbf{v}}^{-1} \mathbf{H})^{-1}$. where, * is complex conjugate.

3.1. Dual basis in state-space models

The results presented in Lemma 2 as a dual basis are used in the following linear stochastic model.

$$\begin{cases} \mathbf{x}_{i+1} = \mathbf{F}_i \mathbf{x}_i + \mathbf{G}_i \mathbf{z}_i, \mathbf{x}_0 = 0 \\ \mathbf{y}_i = \mathbf{H}_i \mathbf{x}_i + \mathbf{D}_i \mathbf{z}_i + \mathbf{v}_i \end{cases} \quad i \ge 0$$
(21)

where \mathbf{F}_i , \mathbf{G}_i , \mathbf{H}_i and \mathbf{D}_i are system matrices; the measurement noise vector \mathbf{v}_i , and the input vector \mathbf{z}_i are modeled as uncorrelated noises with variances $\{\mathbf{Q}_i, \mathbf{R}_i\}$. So that, $\mathbf{R}_z = \|\mathbf{z}\|^2 = \operatorname{diag} \{\mathbf{Q}_0, \mathbf{Q}_1, \dots, \mathbf{Q}_N\}$ and $\mathbf{R}_v = \|\mathbf{v}\|^2 = \operatorname{diag} \{\mathbf{R}_0, \mathbf{R}_1, \dots, \mathbf{R}_N\}$. The state-space model of Eq. (21) creates a linear equation between aggregate of the vectors $\{\mathbf{y}, \mathbf{z}, \mathbf{v}\}$ as:

$$\begin{aligned} & \mathbf{y} \triangleq \operatorname{col} \left\{ \mathbf{y}_0, \dots, \mathbf{y}_{\mathcal{N}} \right\} \\ & \mathbf{z} \triangleq \operatorname{col} \left\{ \mathbf{z}_0, \dots, \mathbf{z}_{\mathcal{N}} \right\} \\ & \mathbf{v} \triangleq \operatorname{col} \left\{ \mathbf{v}_0, \dots, \mathbf{v}_{\mathcal{N}} \right\} \end{aligned}$$
 (22)

By solving and replacing first line of Eq. (21) into the second line, the outputs are obtained. With considering $\mathbf{y}_1, \dots, \mathbf{y}_N$ and aggregating outputs in the form of $\mathbf{y} \triangleq \operatorname{col} \{\mathbf{y}_0, \dots, \mathbf{y}_N\}$, we have:

$$\mathbf{y} = A\mathbf{z} + \mathbf{v}$$

$$\mathbf{A} = \begin{bmatrix}
\mathbf{D}_{0} & 0 & 0 & 0 & 0 & 0 \\
\mathbf{H}_{1}\mathbf{G}_{0} & \mathbf{D}_{1} & 0 & 0 & 0 \\
\mathbf{H}_{2}\mathbf{F}_{1}\mathbf{G}_{0} & \mathbf{H}_{2}\mathbf{G}_{1} & \mathbf{D}_{2} & 0 & 0 \\
\vdots & \vdots & \vdots & \ddots & 0 \\
\mathbf{H}_{N}\mathbf{\Phi}(N, 1)\mathbf{G}_{0} & \mathbf{H}_{N}\mathbf{\Phi}(N, 2)\mathbf{G}_{1} & \dots & \mathbf{H}_{N}\mathbf{G}_{N-1} & \mathbf{D}_{N}
\end{bmatrix}$$
(24)

So that \mathbf{A} is a block lower triangular matrix and $\Phi(\mathbb{N}, i) = \mathbf{F}_{\mathcal{N}-1}\mathbf{F}_{\mathcal{N}-2}\dots\mathbf{F}_i$ [34]. According to Lemma 2, the vectors $\{\mathbf{z}^d, \mathbf{y}^d\}$ that define the dual basis of $\mathcal{L}\{\mathbf{z}, \mathbf{y}\}$ satisfy the relation:

$$\mathbf{z}^d = -\mathbf{A}^* \mathbf{y}^d + \mathbf{v}^d \tag{25}$$

3.2. The equivalent of stochastic and deterministic problems

The projection of **z** on \mathcal{L} {**y**}for the linear model in Eq. (18) is shown with $\hat{\mathbf{z}}_{|\mathbf{y}}$, which can be computed by $\hat{\mathbf{z}}_{|\mathbf{y}} = \mathbf{K}_{o}\mathbf{y}$. So, \mathbf{K}_{o} of the stochastic problem in Eq. (21) is obtained as:

$$\min_{\mathbf{K}} \|\mathbf{z} - \mathbf{K}\mathbf{y}\|^{2}
\mathbf{K}_{o} = \mathbf{R}_{zv} \mathbf{R}_{v}^{-1}$$
(26)

With considering Lemma 2, can be shown that $K_o = (R_z^{-1} + H^*R_v^{-1}H)^{-1}H^*R_v^{-1}$. Another solution of K_o can be obtained by solving the problem of the equivalent deterministic least-square. Now, the deterministic problem for a linear system is considered

$$\begin{cases} \mathbf{x}_{i+1} = \mathbf{F}_i \mathbf{x}_i + \mathbf{G}_i \mathbf{u}_i, & \mathbf{x}(0) = 0 \\ \mathbf{y}_i = \mathbf{H}_i \mathbf{x}_i + \mathbf{v}_i \end{cases}$$
 (27)

According to Eqs. (22) and (23), the deterministic problems can be considered as $\mathbf{y} = \mathbf{H}\mathbf{z} + \mathbf{v}$ [34]. In the deterministic system, Eq. (27), $\hat{\mathbf{z}}$ has the same result of $\hat{\mathbf{z}}_{|\mathbf{y}}$ in the stochastic system, Eq. (21). Therefore, according to the deterministic observations and matrix \mathbf{H} , the problem of determining the vector $\hat{\mathbf{z}}$ is achieved as follows

$$\min_{z} \left[z^* R_z^{-1} z + \| y - Hz \|_{R_z^{-1}}^2 \right]$$
 (28)

Solution of Eq. (28) yields [34]:

$$\hat{\mathbf{z}} = (\mathbf{R}_z^{-1} + \mathbf{H}^* \mathbf{R}_v^{-1} \mathbf{H})^{-1} \mathbf{H}^* \mathbf{R}_v^{-1} \mathbf{y} \triangleq \mathbf{K}_o \mathbf{y}$$
 (29)

Since K_0 is the result of both Eqs. (26) and (28), the stochastic problem of Eq. (26) is considered equivalent to deterministic problem of Eq. (28). Therefore, owing to the duality of linear model of Eqs. (18) and (20), also, through the following stochastic optimization problem, K_0^d is obtained:

$$\min_{\mathbf{K}^d} \|\mathbf{y}^d - \mathbf{K}^d \mathbf{z}^d\|^2
\mathbf{K}_o^d = \mathbf{R}_{y^d z^d} \mathbf{R}_{z^d}^{-1}$$
(30)

ISA Transactions xxx (xxxx) xxx

With considering Lemma 2, K_0^d is obtained as:

$$\mathbf{K}_{o}^{d} = -\mathbf{R}_{v}^{-1}\mathbf{H}(\mathbf{R}_{z}^{-1} + \mathbf{H}^{*}\mathbf{R}_{v}^{-1}\mathbf{H})^{-1}$$
(31)

With considering the following optimal deterministic problem:

$$\min_{\boldsymbol{v}^d} \left[\boldsymbol{y}^{d*} \boldsymbol{R}_v \boldsymbol{y}^d + \left\| \boldsymbol{z}^d + \boldsymbol{H}^* \boldsymbol{y}^d \right\|_{\boldsymbol{R}_z}^2 \right]$$
 (32)

and solving for $\hat{\boldsymbol{y}}^d$ gives:

$$\hat{\boldsymbol{y}}^d = -(\boldsymbol{R}_v + \boldsymbol{H}\boldsymbol{R}_z\boldsymbol{H}^*)^{-1}\boldsymbol{H}\boldsymbol{R}_z\boldsymbol{z}^d \triangleq \boldsymbol{K}_o^d\boldsymbol{z}^d$$
(33)

Comparing the optimal problem Eqs. (26) and (30), it can be concluded that $\mathbf{K}_o^d = -\mathbf{K}_o^*$. Therefore, Eqs. (26) and (30) are dual, and the gains of the corresponding matrices are each other's negative conjugate transpose.

3.2.1. Duality via deterministic optimal problem solving

The following discrete-time deterministic optimization problem with constraint $\mathbf{x}_{i+1} = \mathbf{F}_i \mathbf{x}_i + \mathbf{G}_i \mathbf{u}_i$ and $\mathbf{x}(0) = 0$ of Eq. (27) is considered:

$$\min_{\{\boldsymbol{u}_{0},...,\boldsymbol{u}_{N}\}} \left[\boldsymbol{x}_{N+1}^{*} \boldsymbol{S}_{N+1}^{d} \boldsymbol{x}_{N+1} + \sum_{i=1}^{N} (\boldsymbol{y}_{i} - \boldsymbol{H}_{i} \boldsymbol{x}_{i})^{*} \boldsymbol{R}_{i}^{d} (\boldsymbol{y}_{i} - \boldsymbol{H}_{i} \boldsymbol{x}_{i}) + \sum_{i=0}^{N} \boldsymbol{u}_{i}^{*} \boldsymbol{Q}_{i}^{d} \boldsymbol{u}_{i} \right]$$
(34)

where \cdot^* stands for Hermitian transposition, and $S_{N+1}^d \geq 0$, $R_i^d \geq 0$ and $Q_i^d > 0$ are weighting matrices [34]. The problem of the deterministic optimization in Eq. (34) can be expressed in the form of Eq. (28). By solving the optimization problem with consideration of the dual theory, the stochastic optimization problem is solved. For this purpose, the vectors $\mathbf{u} = \text{col}\{\mathbf{u}_0, \mathbf{u}_1, \dots, \mathbf{u}_N\}$ and $\mathbf{s} = \text{col}\{\mathbf{u}_0, \mathbf{u}_1, \mathbf{u}_1, \dots, \mathbf{u}_N\}$, and also the block lower triangular matrix are introduced as:

$$\mathbf{B}_{d} = \begin{bmatrix} \Phi(\mathcal{N}+1,1)\mathbf{G}_{0} & \Phi(\mathcal{N}+1,2)\mathbf{G}_{1} & \dots & \Phi(\mathcal{N}+1,\mathcal{N})\mathbf{G}_{\mathcal{N}-1} & \mathbf{G}_{\mathcal{N}} \\ 0 & & & & \\ \mathbf{H}_{1}\mathbf{G}_{0} & 0 & & & & \\ \mathbf{H}_{2}\Phi(2,1)\mathbf{G}_{0} & \mathbf{H}_{2}\mathbf{G}_{1} & 0 & & & \\ \vdots & \vdots & \ddots & 0 & & & \\ \mathbf{H}_{\mathcal{N}}\Phi(\mathcal{N},1)\mathbf{G}_{0} & \mathbf{H}_{\mathcal{N}}\Phi(\mathcal{N},2)\mathbf{G}_{1} & \dots & \mathbf{H}_{\mathcal{N}}\mathbf{G}_{\mathcal{N}-1} & 0 \end{bmatrix}$$
(35)

By direct calculations, the following equation is obtained [34]:

$$\begin{bmatrix} \mathbf{x}_{N+1} \\ \mathbf{s} \end{bmatrix} = \mathbf{B}_d \mathbf{u} \tag{36}$$

Therefore, Eq. (34) is rewritten as:

$$\min_{\mathbf{u}} \left[\mathbf{u}^* \mathbf{Q}^d \mathbf{u} + \left\| \begin{bmatrix} 0 \\ -\mathbf{y} \end{bmatrix} + \mathbf{B}_d \mathbf{u} \right\|_{\mathbf{W}^d}^2 \right]$$
 (37)

where $\mathbf{y} = \operatorname{col} \left\{ \mathbf{y}_0, \mathbf{y}_1, \dots, \mathbf{y}_{\scriptscriptstyle N} \right\}$, $\mathbf{W}^d \triangleq \operatorname{diag} \left\{ \mathbf{S}^d_{\scriptscriptstyle N+1}, \mathbf{R}^d_0, \dots, \mathbf{R}^d_{\scriptscriptstyle N} \right\}$ and $\mathbf{Q}^d \triangleq \operatorname{diag} \left\{ \mathbf{Q}^d_0, \dots, \mathbf{Q}^d_{\scriptscriptstyle N} \right\}$. Eq. (37) is another form of Eq. (28), and the matrix coefficient obtained from solution of Eq. (37) is expressed as:

$$\hat{\boldsymbol{u}} = \boldsymbol{K}_o \begin{bmatrix} 0 \\ -\boldsymbol{y} \end{bmatrix} \tag{38}$$

Therefore, the optimal matrix K_0 is determined by the projection of \mathbf{y}^d on \mathbf{z}^d in the stochastic dual model [26].

$$\mathbf{z}^d = \mathbf{B}_d^* \mathbf{y}^d + \mathbf{v}^d \tag{39}$$

where $\{\mathbf{y}^d, \mathbf{v}^d\}$ is uncorrelated with the variances $\|\mathbf{y}^d\|^2 = \mathbf{W}^d$ and $\|\mathbf{v}^d\|^2 = \mathbf{Q}^d$.

In the following, a time-varying linear control method based on hybrid functions is designed and accordingly, the dual observer gain is obtained. In this paper, since the elements of $\dot{\mathbf{x}}(t)$ and $\mathbf{u}(t)$ are expanded as hybrid Legendre polynomials and blockpulse function, the system dynamics is converted to algebraic equations with unknown coefficients.

3.3. Properties of hybrid functions

The following hybrid functions $b_{nm}(t)$, $m=0,1,\ldots,M-1, n=1,2,\ldots,N$ are defined in the interval $0 \le t < t_f$ with m,n and t being the order of Legendre polynomials, block-pulse functions and normalized time.

$$b_{nm}(t) = \begin{cases} P_m\left(\frac{2N}{t_f}t - 2n + 1\right), & \left(\frac{n-1}{N}\right)t_f \le t < \frac{n}{N}t_f\\ 0, & \text{otherwise} \end{cases}$$
(40)

where, the Legendre polynomial $P_m(t)$ is defined as:

$$P_{0}(t) = 1$$

$$P_{1}(t) = t$$

$$P_{m+1}(t) = \left(\frac{2m+1}{m+1}\right) t P_{m}(t)$$

$$-\left(\frac{m}{m+1}\right) P_{m-1}(t), m = 1, 2, 3, ...$$
(41)

Using hybrid functions [35], each term f(t) is approximated in the interval $0 \le t < t_f$ as follows:

$$f(t) \cong \sum_{n=1}^{N} \sum_{m=0}^{M-1} c_{nm} b_{nm}(t) = \mathbf{c}^{T} \mathbf{b}(t)$$

$$(42)$$

where

$$\mathbf{c} = [c_{10}, \dots, c_{1M-1}, c_{20}, \dots, c_{2M-1}, \dots, c_{N0}, \dots, c_{NM-1}]^T$$
 (43)

and

$$\mathbf{b}(t) = [b_{10}(t), \dots, b_{1M-1}(t), b_{20}(t), \dots, b_{2M-1}(t), \dots, b_{N0-1}(t)]^{T}$$

$$(44)$$

where c and b(t) are of dimension $MN \times 1$. The integration of vector b(t) is approximated as:

$$\int_{0}^{t} \boldsymbol{b}\left(t'\right) dt' \simeq \boldsymbol{P}\boldsymbol{b}(t) \tag{45}$$

where the integral operational block matrix P of dimension $MN \times MN$ is defined as [36]:

$$P = \begin{bmatrix} E & L & L & \cdots & L \\ O & E & L & \cdots & L \\ O & O & E & \cdots & L \\ \vdots & \vdots & \vdots & & \vdots \\ O & O & O & \cdots & E \end{bmatrix}$$
(46)

in which **0** denotes zero matrix of compatible dimensions, and $M \times M$ matrix **L** is defined as:

$$L = \frac{t_f}{N} \begin{bmatrix} 1 & 0 & 0 & \cdots & 0 \\ 0 & 0 & 0 & \cdots & 0 \\ 0 & 0 & 0 & \cdots & 0 \\ \vdots & \vdots & \vdots & & \vdots \\ 0 & 0 & 0 & \cdots & 0 \end{bmatrix}$$

$$(47)$$

ISA Transactions xxx (xxxx) xxx

similarly, \mathbf{E} is a $M \times M$ matrix defined as:

$$\mathbf{E} = \frac{t_f}{N} \begin{bmatrix} 1 & 1 & 0 & 0 & \dots & 0 & 0 & 0 \\ -1/3 & 0 & 1/3 & 0 & \dots & 0 & 0 & 0 \\ 0 & -1/5 & 0 & 1/5 & \dots & 0 & 0 & 0 \\ \vdots & \vdots & \vdots & \vdots & & \vdots & \vdots & \vdots \\ 0 & 0 & 0 & 0 & \dots & \frac{-1}{2M-3} & 0 & \frac{1}{2M-3} \\ 0 & 0 & 0 & 0 & \dots & 0 & \frac{-1}{2M-1} & 0 \end{bmatrix}$$

$$(48)$$

Property 1. The product of two hybrid functions is represented as [37]:

$$\boldsymbol{b}(t)\,\boldsymbol{b}^{\mathrm{T}}(t)\,\boldsymbol{c} \simeq \tilde{\boldsymbol{C}}\boldsymbol{b}(t) \tag{49}$$

where $\tilde{\mathbf{C}}$ is a MN × MN product operational matrix.

3.4. State-space model for linear system

Continuous time-varying model of system Eq. (27) is considered here:

$$\begin{cases} \dot{\boldsymbol{x}}(t) = \boldsymbol{F}(t) \, \boldsymbol{x}(t) + \boldsymbol{G}(t) \, \boldsymbol{u}(t), \, \boldsymbol{x}(0) = \boldsymbol{x}_0 \\ \boldsymbol{y}(t) = \boldsymbol{H}(t) \, \boldsymbol{x}(t) + \boldsymbol{v} \end{cases}$$
(50)

where $\mathbf{x}(t) \in \mathbb{R}^l$, $\mathbf{u}(t) \in \mathbb{R}^q$, $\mathbf{y}(t) \in \mathbb{R}^e$, and $\mathbf{x}(0)$ are state, control input, measurement and initialization vectors together with system matrix $\mathbf{F}(t)$, input distribution matrix $\mathbf{G}(t)$ and measurement matrix $\mathbf{H}(t)$. In order to obtain control input $\mathbf{u}(t)$, the following cost function J must be minimized to the corresponding state trajectory of $\mathbf{x}(t)$ in the interval $0 \le t < t_f$:

$$J = \frac{1}{2} \mathbf{x}^{T} \left(t_{f} \right) \mathbf{S} \mathbf{x} \left(t_{f} \right) + \frac{1}{2} \int_{0}^{t_{f}} \left[\mathbf{x}^{T} \left(t \right) \mathbf{R} \left(t \right) \mathbf{x} \left(t \right) + \mathbf{u}^{T} \left(t \right) \mathbf{Q} \left(t \right) \mathbf{u} \left(t \right) \right] dt$$

$$(51)$$

with T showing transposition of matrix.

3.5. Approximation of state equations with using hybrid functions

The dynamical system introduced in Eq. (50) is approximated to:

$$\dot{\boldsymbol{x}}(t) = \left[\dot{\boldsymbol{x}}_1(t), \dot{\boldsymbol{x}}_2(t), \dots, \dot{\boldsymbol{x}}_l(t)\right]^T \tag{52}$$

$$\boldsymbol{u}(t) = \left[\boldsymbol{u}_1(t), \boldsymbol{u}_2(t), \dots, \boldsymbol{u}_q(t)\right]^T$$
 (53)

$$\mathbf{y}(t) = \left[\mathbf{y}_1(t), \mathbf{y}_2(t), \dots, \mathbf{y}_e(t)\right]^T \tag{54}$$

$$\hat{\boldsymbol{b}}(t) = \boldsymbol{I}_l \otimes \boldsymbol{b}(t) \tag{55}$$

$$\hat{\boldsymbol{b}}_1(t) = \boldsymbol{I}_a \otimes \boldsymbol{b}(t) \tag{56}$$

$$\hat{\boldsymbol{b}}_{2}(t) = \boldsymbol{I}_{e} \otimes \boldsymbol{b}(t) \tag{57}$$

where $\emph{\textbf{I}}_l$, $\emph{\textbf{I}}_q$ and $\emph{\textbf{I}}_e$ are identity matrices of dimensions $l \times l$, $q \times q$ and $e \times e$, respectively. Also, \otimes denotes Kronecker product [38]. By use of the Kronecker product properties, $\hat{\emph{\textbf{b}}}(t)$, $\hat{\emph{\textbf{b}}}_1(t)$ and $\hat{\emph{\textbf{b}}}_2(t)$ are vectors of dimensions $lMN \times l$, $qMN \times q$ and $eMN \times e$, respectively. Consequently:

$$\dot{\boldsymbol{x}}(t) = \hat{\boldsymbol{b}}^T(t)\,\boldsymbol{x} \tag{58}$$

$$\boldsymbol{u}(t) = \hat{\boldsymbol{b}}_{1}^{T}(t)\,\boldsymbol{u} \tag{59}$$

$$\mathbf{y}(t) = \hat{\mathbf{b}}_{2}^{\mathrm{T}}(t)\mathbf{y} \tag{60}$$

Order for \boldsymbol{x} , \boldsymbol{u} and \boldsymbol{y} vectors are $lMN \times 1$, $qMN \times 1$ and $eMN \times 1$, respectively:

$$\mathbf{x} = [\mathbf{x}_1, \mathbf{x}_2, \dots, \mathbf{x}_l]^T \tag{61}$$

$$\mathbf{u} = \begin{bmatrix} \mathbf{u}_1, \mathbf{u}_2, \dots, \mathbf{u}_q \end{bmatrix}^T \tag{62}$$

Also

$$\boldsymbol{y} = [\boldsymbol{y}_1, \boldsymbol{y}_2, \dots, \boldsymbol{y}_e]^T \tag{63}$$

Similarly,

$$\mathbf{x}(0) = \hat{\mathbf{b}}^{T}(t) \, \mathbf{d} \tag{64}$$

where $\mathbf{d} = [\mathbf{d}_1, \mathbf{d}_2, \dots, \mathbf{d}_l]^T$ is a vector of order $lMN \times 1$. In Eq. (58), by integrating from 0 to t, we have:

$$\mathbf{x}(t) - \mathbf{x}(0) = \int_{0}^{t} \hat{\mathbf{b}}^{T}(t') \mathbf{x} dt'$$

$$= (\mathbf{I}_{l} \otimes \mathbf{b}^{T}(t)) (\mathbf{I}_{l} \otimes \mathbf{P}^{T}) \mathbf{x} = \hat{\mathbf{b}}^{T}(t) \hat{\mathbf{P}}^{T} \mathbf{x}$$
(65)

The matrix P is defined by Eq. (45). Using Eqs. (64) and (65) we have:

$$\mathbf{x}(t) = \hat{\mathbf{b}}^{T}(t)(\mathbf{d} + \hat{\mathbf{P}}^{T}\mathbf{x}) \tag{66}$$

With use of the hybrid function, F(t) and G(t) can be written as follows:

$$\mathbf{F}(t) = [F_{10}, F_{11}, \dots, F_{1M-1}, \dots, F_{N0}, F_{N1}, \dots, F_{NM-1}] \hat{\mathbf{b}}(t) = \mathbf{F}^T \hat{\mathbf{b}}(t)$$
(67)

$$\mathbf{G}(t) = [G_{10}, G_{11}, \dots, G_{1M-1}, \dots, G_{N0}, G_{N1}, \dots, G_{NM-1}] \,\hat{\mathbf{b}}(t) = \mathbf{G}^{\mathsf{T}} \,\hat{\mathbf{b}}_{1}(t)$$
(68)

$$\mathbf{H}(t) = [H_{10}, H_{11}, \dots, H_{1M-1}, \dots, H_{N0}, H_{N1}, \dots, H_{NM-1}] \hat{\mathbf{b}}(t)$$

$$= \mathbf{H}^T \hat{\mathbf{b}}_2(t)$$
(69)

where \mathbf{F}^T , \mathbf{G}^T and \mathbf{H}^T are of dimensions $l \times lMN$, $l \times qMN$ and $l \times eMN$, respectively. Therefore:

$$\mathbf{F}(t)\mathbf{x}(t) = \mathbf{F}^{T}\hat{\mathbf{b}}(t)\hat{\mathbf{b}}^{T}(t)\left(\mathbf{d} + \hat{\mathbf{P}}^{T}\mathbf{x}\right) = \hat{\mathbf{b}}^{T}(t)\tilde{\mathbf{F}}^{T}\left(\mathbf{d} + \hat{\mathbf{P}}^{T}\mathbf{x}\right)$$
(70)

$$\boldsymbol{G}(t)\boldsymbol{u}(t) = \boldsymbol{G}^{T}\hat{\boldsymbol{b}}_{1}(t)\hat{\boldsymbol{b}}_{1}^{T}(t)\boldsymbol{u} = \hat{\boldsymbol{b}}^{T}(t)\tilde{\boldsymbol{G}}^{T}\boldsymbol{u}$$
(71)

$$\boldsymbol{H}(t)\boldsymbol{x}(t) = \boldsymbol{H}^{T}\hat{\boldsymbol{b}}_{2}(t)\hat{\boldsymbol{b}}^{T}(t)\left(\boldsymbol{d} + \hat{\boldsymbol{P}}^{T}\boldsymbol{x}\right)$$
(72)

By use of Property 1, \tilde{F} and \tilde{G} can be calculated. Therefore, the state-space model of Eq. (50) is rewritten as:

$$\hat{\boldsymbol{b}}^{T}(t)\boldsymbol{x} = \hat{\boldsymbol{b}}^{T}(t)\tilde{\boldsymbol{F}}^{T}(\boldsymbol{d} + \hat{\boldsymbol{P}}^{T}\boldsymbol{x}) + \hat{\boldsymbol{b}}^{T}(t)\tilde{\boldsymbol{G}}^{T}\boldsymbol{u}$$
(73)

So, we will have:

$$\left(\tilde{\boldsymbol{F}}^{T}\hat{\boldsymbol{P}}^{T} - \boldsymbol{I}\right)\boldsymbol{x} + \tilde{\boldsymbol{G}}^{T}\boldsymbol{u} + \tilde{\boldsymbol{F}}^{T}\boldsymbol{d} = 0$$
(74)

3.6. Approximation of cost functions using hybrid functions

With substituting Eqs. (59) and (66) in Eq. (51), we have:

$$J = \frac{1}{2} \left(\boldsymbol{d} + \hat{\boldsymbol{P}}^{T} \boldsymbol{x} \right)^{T} \hat{\boldsymbol{b}} \left(t_{f} \right) \boldsymbol{S} \hat{\boldsymbol{b}}^{T} \left(t_{f} \right) \left(\boldsymbol{d} + \hat{\boldsymbol{P}}^{T} \boldsymbol{x} \right)$$

$$+ \frac{1}{2} \left(\boldsymbol{d} + \hat{\boldsymbol{P}}^{T} \boldsymbol{x} \right)^{T} \left[\int_{0}^{t_{f}} \hat{\boldsymbol{b}} \left(t \right) \boldsymbol{R} (t) \hat{\boldsymbol{b}}^{T} \left(t \right) dt \right] \left(\boldsymbol{d} + \hat{\boldsymbol{P}}^{T} \boldsymbol{x} \right)$$

$$+ \frac{1}{2} \boldsymbol{u}^{T} \left[\int_{0}^{t_{f}} \hat{\boldsymbol{b}}_{1} \left(t \right) \boldsymbol{Q} (t) \hat{\boldsymbol{b}}_{1}^{T} \left(t \right) dt \right] \boldsymbol{u}$$

$$(75)$$

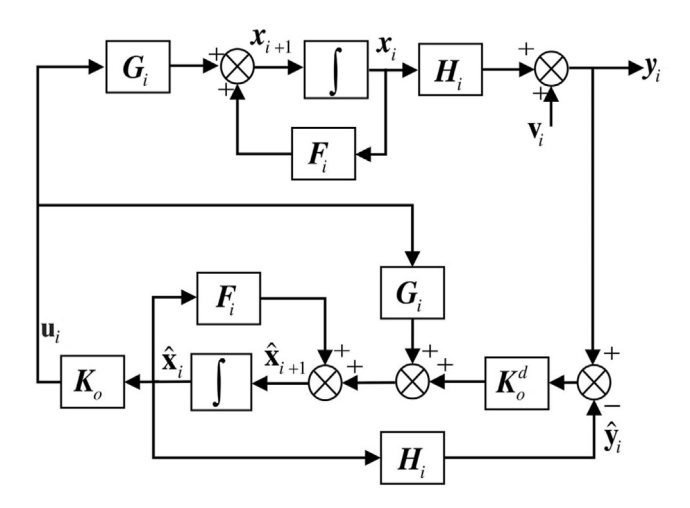


Fig. 3. Duality in state-space model between observer and control [26,39].

Which is simplified as follows:

$$J = \frac{1}{2} \left(\mathbf{d} + \hat{\mathbf{P}}^{T} \mathbf{x} \right)^{T} \left(\mathbf{b} \left(t_{f} \right) \mathbf{b}^{T} \left(t_{f} \right) \otimes \mathbf{S} \right) \left(\mathbf{d} + \hat{\mathbf{P}}^{T} \mathbf{x} \right)$$

$$+ \frac{1}{2} \left(\mathbf{d} + \hat{\mathbf{P}}^{T} \mathbf{x} \right)^{T} \left(\mathbf{L}_{M} \otimes \mathbf{R} \right) \left(\mathbf{d} + \hat{\mathbf{P}}^{T} \mathbf{x} \right) + \frac{1}{2} \mathbf{u}^{T} \left(\mathbf{L}_{M} \otimes \mathbf{Q} \right) \mathbf{u}$$

$$(76)$$

$$\mathbf{L}_{\mathbf{M}} = \int_{0}^{t_{f}} \left(\mathbf{b}(t) \, \mathbf{b}^{\mathsf{T}}(t) \right) \mathrm{d}t \tag{77}$$

Eq. (75) yields a diagonal matrix as:

$$L_{\mathbf{M}} = \begin{bmatrix} \mathbf{T} & \mathbf{O} & \dots & \mathbf{O} \\ \mathbf{O} & \mathbf{T} & \dots & \mathbf{O} \\ \vdots & \vdots & \ddots & \vdots \\ \mathbf{O} & \mathbf{O} & & \mathbf{T} \end{bmatrix}$$
(78)

where \mathfrak{T} is a diagonal block matrix with dimension $M \times M$.

$$\tau = \frac{t_f}{N} \begin{bmatrix}
1 & 0 & \dots & 0 \\
0 & \frac{1}{3} & \dots & 0 \\
\vdots & \vdots & \ddots & \dots \\
0 & 0 & \vdots & \frac{1}{2M-1}
\end{bmatrix}$$
(79)

The following equation is used to minimize the cost function of Eq. (76) considering Eq. (50):

$$L(\mathbf{x}, \mathbf{u}, \lambda) = J(\mathbf{x}, \mathbf{u}) + \lambda^{T} \left[\left(\tilde{\mathbf{F}}^{T} \hat{\mathbf{p}}^{T} - \mathbf{I} \right) \mathbf{x} + \tilde{\mathbf{G}}^{T} \mathbf{u} + \tilde{\mathbf{F}}^{T} \mathbf{d} \right]$$
(80)

where λ shows Lagrange multipliers. Therefore, the following equations are obtained:

$$\begin{cases} \frac{\partial L(\mathbf{x}, \mathbf{u}, \lambda)}{\partial \mathbf{x}} = 0\\ \frac{\partial L(\mathbf{x}, \mathbf{u}, \lambda)}{\partial \mathbf{u}} = 0\\ \frac{\partial L(\mathbf{x}, \mathbf{u}, \lambda)}{\partial \lambda} = 0 \end{cases}$$
(81)

Solution of Eqs. (81) yields \mathbf{x} and \mathbf{u} and the gain matrix in deterministic system is obtained by $\mathbf{u} = \mathbf{K}_0 \begin{bmatrix} 0 \\ -\mathbf{x} \end{bmatrix}$. In Fig. 3, the block diagram of the dual estimation and control systems is shown [26,39].



Fig. 4. Test equipment comprising Vitans system, ADIS-16407, and Garmin-35.

According to the block diagram of Fig. 3 and Eqs. (70) to (72), the recursive BPLPO observer equations are resulted as:

$$\begin{cases}
\hat{\mathbf{x}}_{i+1} = \hat{\mathbf{b}}^{T}(t) \tilde{\mathbf{F}}^{T} \left(\mathbf{d} + \hat{\mathbf{P}}^{T} \hat{\mathbf{x}}_{i} \right) + \hat{\mathbf{b}}^{T}(t) \tilde{\mathbf{G}}^{T} \mathbf{u}_{i} \\
+ \mathbf{K}_{o}^{d} \left(\mathbf{H}^{T} \hat{\mathbf{b}}_{2}(t) \hat{\mathbf{b}}^{T}(t) \left(\mathbf{d} + \hat{\mathbf{P}}^{T} \mathbf{x}_{i} \right) - \hat{\mathbf{y}}_{i} \right) \\
\hat{\mathbf{y}}_{i} = \mathbf{H}^{T} \hat{\mathbf{b}}_{2}(t) \hat{\mathbf{b}}^{T}(t) \left(\mathbf{d} + \hat{\mathbf{P}}^{T} \hat{\mathbf{x}}_{i} \right)
\end{cases} (82)$$

where, the observer gain matrix \mathbf{K}_o^d to estimate the state vector as, $\hat{\mathbf{x}}_i$ is obtained by comparing Eqs. (26) and (30) as $\mathbf{K}_o^d = -\mathbf{K}_o^*$.

4. Experimental results and discussion

In the following, the performance of the designed BPLPO in earlier Section 3 is practically assessed through various maneuvers of a ground vehicle. The results obtained from the new BPLPO are compared with those of the EKF. A reference Vitans INS/ GPS involving triple gyroscopes, accelerometers, magnetometers, together with a barometric altimeter and temperature sensor should produce relatively accurate data. Moreover, the low-cost AHRS board of BPLPO is equipped with 1 Hz Garmin 35 GPS receiver, HMC1022 magnetic compass and ADIS16407 IMU under 50 Hz data sampling frequency. The features of HMC1022 magnetometers and ADIS16407 module are listed in Table 1 [31]. Fig. 4 shows the strapped Vitans system, GPS, ADIS16407 and other sensors board on the test vehicle. Through standard RS-232 serial port connected via a Laptop, online data monitoring of raw sensors and estimation filter outputs are carried out. To attenuate hard- and soft-iron magnetic disturbances impacting on the TAM, the pack of sensors are fixed on a solid aluminum profile.

The flowchart of the estimation process of the roll, pitch, and heading angles inside the AHRS system is depicted in Fig. 5. According to the swinging algorithm of Fig. 2, the AHRS raw sensors and filtered data during the first 5 s of the test were used for calibration purpose of the TAM. Therefore, the calibration coefficients a through e are imposed on the TAM data to produce calibrated heading angle online. In the AHRS system, the accelerometers and calibrated heading angle data are used along with GPS data to correct non-gravity accelerations as much as possible [25,26].

Table 1Inertial-Magnetic Sensors specifications [31].

Sensor	Model	Full-scale (FS) range	Noise density	Bias stability	Initial bias error $\pm 1\sigma$	Nonlinearity (%FS)
Gyroscope	ADXRS150	±150°/s	$0.05^{\circ}/s/\sqrt{Hz}$	0.01°/s	±3°/s	0.1
Accelerometer (single-axis)	ADXL202	$\pm 20^{\circ} \text{m/s}^2$	0.01 m/s^2	0.05 m/s^2	± 0.02 g	0.2
Accelerometer (dual-axis)	ADXL210E	$\pm 100 \text{ m/s}^2$	0.01m/s^2	0.05 m/s^2	± 0.02 g	0.2
Magnetometer	HMC1022	$\pm 200~\mu T$	$10^{-5} \mu T/\sqrt{Hz}$	0.01 μΤ	$2\times 10^{-5}~\mu T$	0.1

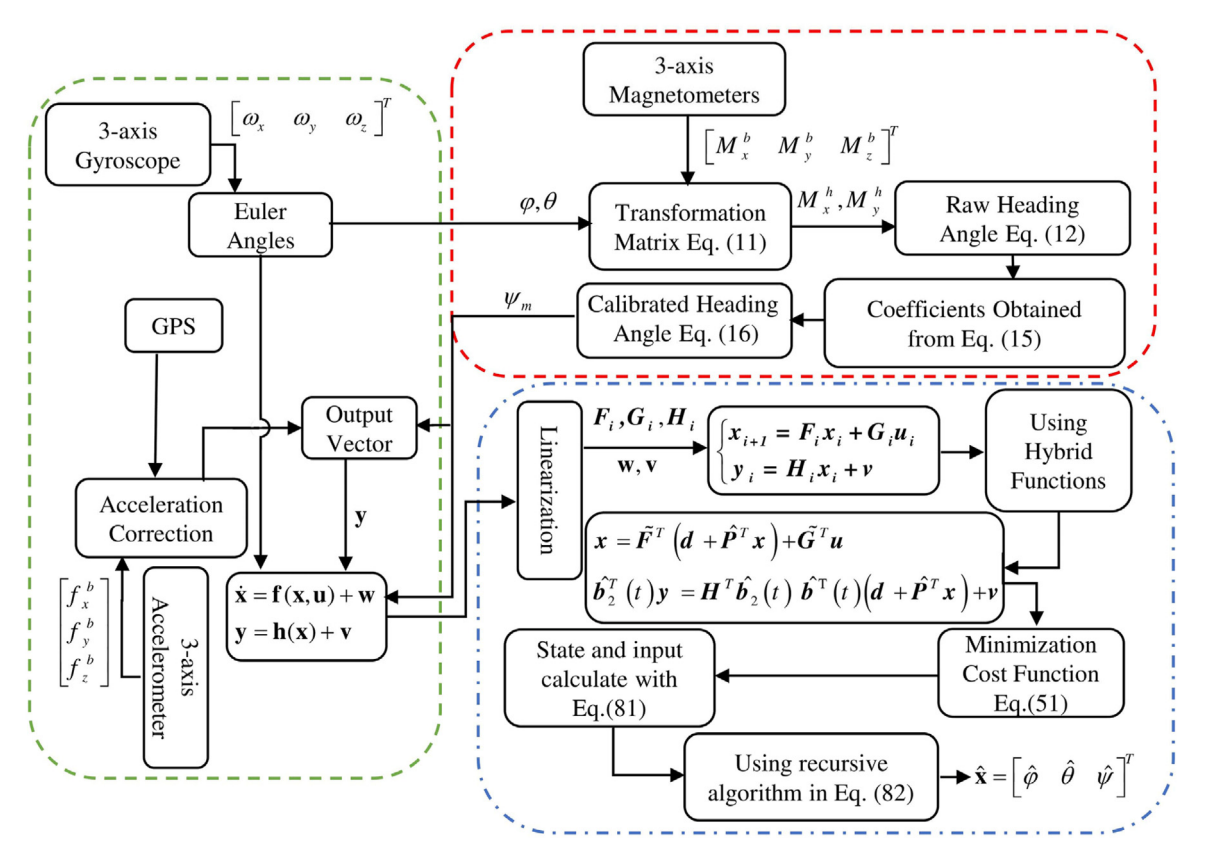


Fig. 5. Flowchart for estimating the angles of the AHRS system with the swinging calibration and hybrid functions.

Coriolis and remainder accelerations are considered as 2-norm bounded disturbances whereas the output vector should include merely the gravitational acceleration affecting the vehicle. Table 2 presents the pseudo-code of BPLPO for implementation in the AHRS.

In order to assess the proposed observer, two tests have been performed with different maneuver conditions. The trajectories of tracking vehicle in the N, E, D frame for tests 1 and 2 are shown in Fig. 6. The TAM calibration coefficients for tests No. 1 and No. 2 are computed as Eq. (83), which compensate bias, SF, and disturbance uncertainties. The values of hybrid function parameters are considered, M=2 and N=3.

TestNo.1:
$$\begin{cases} a = 0.1385 \\ b = -0.0275 \\ c = 0.3608 \\ d = 0.3573 \\ e = -0.1172 \\ a = 0.0219 \\ b = 0.0950 \\ c = -0.0479 \\ d = 0.0220 \\ e = -0.0238 \end{cases}$$
 (83)

According to the sensors specification released in factory datasheets together with upper bounds of ground vehicle velocity and position vector, the following aggregated covariance values are implemented in both observers:

$$\mathbf{Q} = \operatorname{diag} \left(1.1 \times 10^{-3}, 1.1 \times 10^{-3}, 1.6 \times 10^{-1} \right) (\operatorname{rad}^{2}/\operatorname{s}^{2})$$

$$\mathbf{R} = \operatorname{diag} \left(0.9, 0.9, 0.5 \right) (\operatorname{rad}^{2})$$
(84)

As the alignment process, at first 55 s of test No. 1 carried out about 580 s, the vehicle was stationary to initialization of state vector and compensation of on–off bias of the gyroscopes. During exhaust of this test, in Figs. 7 and 8 the obtained attitude and heading angles with respect to Vitans system are shown. In Table 3 the mean values (MVs) and standard deviation (SD) of the corresponding errors are gathered.

In Fig. 6, the tracked path curvatures in 550 s of test No. 2 imply execution of various dynamical maneuvers by the test vehicle. Similar to the earlier test No. 1, the vehicle was stationary for about 100 s to alignment and compensation for the on–off bias of sensors. By use of this test, the observer performance compared to the EKF method are shown in Figs. 9 and 10, and the statistical parameters are represented in Table 4.

According to the results obtained in this paper, the EKF propagation of estimation covariance matrix uses the first order of the Taylor series. While high order approximation terms are used in the propagation of estimation equation in this paper.

Table 2BPLPO implementation pseudo-code in AHRS.

```
Require: IMU data (Gyroscopes, Accelerators, GPS, TAM)
Initialization: t = 0, \mathbf{R}, \mathbf{Q}, \hat{\mathbf{x}}_0 = 0
   While t < t_f do
   Set IMU-data\rightarrow \omega_{nh}^b, \int_x^b
   Set GPS-data\rightarrow \psi_{GPS}
   Set TAM-data\rightarrow M_x^b
    \psi_{\text{raw}} \rightarrow \text{Eq. (12)}
       if t < 5 s do
        \delta\psi \rightarrow \text{Eq. (13)}
       Compute a to e with Eq. (15)
       else
       a to e obtained in the previous step should be considered.
       end-if
\psi_m \rightarrow \text{Eq. (16)}
Used GPS-data\rightarrowa<sub>C</sub> with (\omega \times \mathbf{V})
\mathbf{F}_i \rightarrow \mathbf{f}(\mathbf{x}, \mathbf{u}) and Eq. (42)
G_i \rightarrow f(\mathbf{x}, \mathbf{u}) and Eq. (42)
\mathbf{H}_i \rightarrow \mathbf{h}(\mathbf{x}) and Eq. (42)
u, x \rightarrow  Solving Eqs. (81)
K_0 \rightarrow \text{ with } \mathbf{u} = K_0
\hat{\mathbf{x}}_{i+1} \leftarrow \hat{\mathbf{x}}_i with Eq. (82)
\hat{\mathbf{x}}_{i+1} \rightarrow \begin{bmatrix} \hat{\varphi} \end{bmatrix}
                        \hat{\theta}
t = t + dt
end-While
```

Table 3Statistical characteristics of estimation error in test No. 1.

Error signal	PBLPO		EKF	
	MV	SD	MV	SD
φ (°)	0.04	0.89	0.28	1.82
θ (°)	0.06	1.13	-0.54	1.78
ψ (°)	4.54	9.52	4.69	11.13

 Table 4

 Statistical characteristics of estimation error in test No. 2.

Error signal	PBLPO		EKF		
	MV	SD	MV	SD	
φ (°)	0.85	1.84	-2.25	5.60	
θ (°)	-0.09	2.22	-1.57	3.05	
ψ (°)	-5.17	6.59	-5.07	6.57	

Also, instable bias, SF, nonlinearities and other uncertainties of MEMS sensors and nonlinear modeling errors are considered as 2-norm upper bound signals. However, according to the Kalman family filters policy, all the uncertainties and noises should be considered as white Gaussian signals, which are not compatible with the real sensors specification in datasheets.

5. Conclusions

In implementation of MEMS inertial sensors in the AHRS, despite advantages of low-cost and small size, uncertainty of measurements is a main issue. In this paper, to decrease the impact of uncertainties on navigation data, a new linear observer has been designed. Considering the duality theory, it was emphasized that the estimation and control of linear systems are dual. By use of hybrid functions, including Legendre polynomials and block-pulse function, the product and operational matrices of integration on control system equations reduced to solving some algebraic equations. Accordingly, the newly proposed PBLPO was developed based on the dual control system under 2-norm bounded uncertainties and noises. The implemented PBLPO in the AHRS was assessed on a ground vehicle in an urban environment. The orientation Euler angles showed superiority

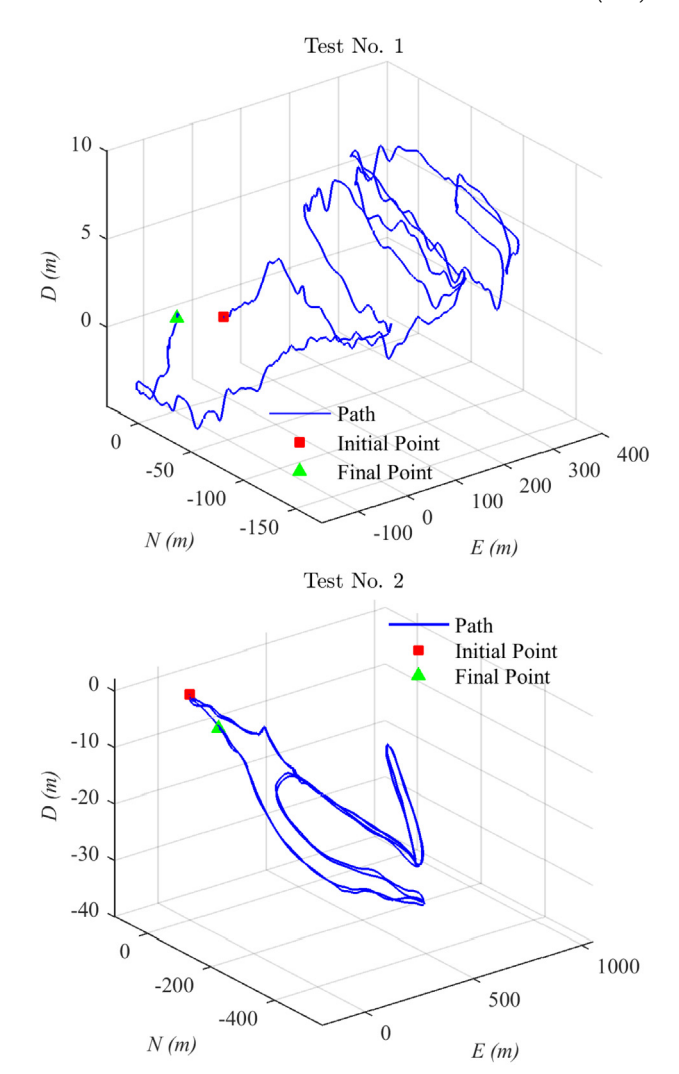


Fig. 6. Vehicles trajectories during tests No. 1 and 2.

of the PBLPO despite its linearity rather than the EKF method. Beyond the KF and EKF, higher order nonlinear Gaussian filters in particular the UKF and CKF request higher order approximations of nonlinear terms in propagation of estimation covariance matrix rather than the first order Taylor expansion. Therefore, by use of hybrid functions, higher order approximation of the covariance matrices may be obtained in the nonlinear filters.

Declaration of competing interest

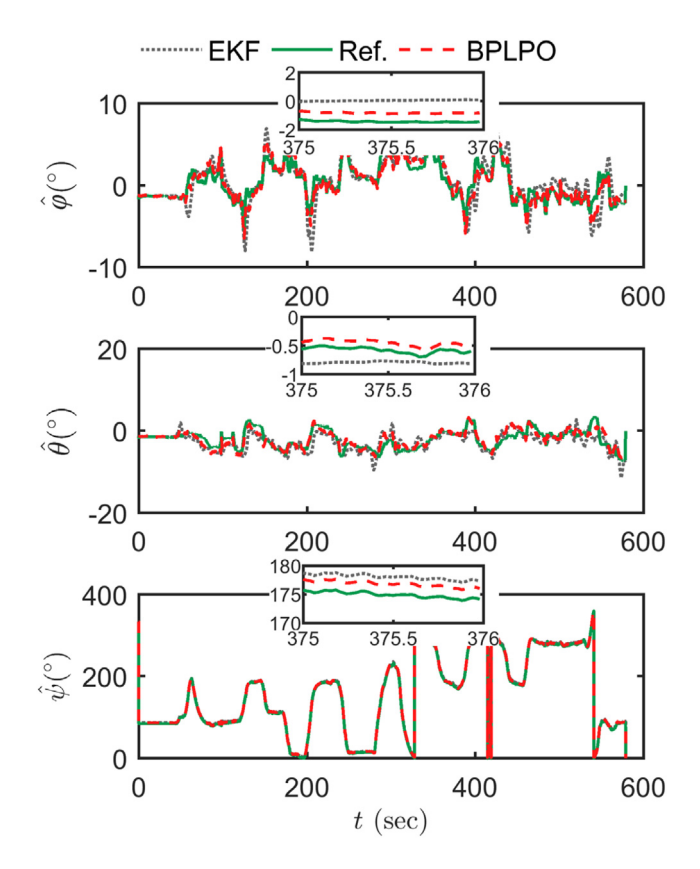
The authors declare that they have no known competing financial interests or personal relationships that could have appeared to influence the work reported in this paper.

Acknowledgments

The authors are grateful to the Iran National Science Foundation (INSF) (No. 97013598) for partial financial support.

Appendix

Definition A.1. In linear algebra, the Gramian matrix is defined by \mathbf{R}_{zy} for a set of vectors $\left\{\mathbf{z}_{i=0,...,\mathcal{M}},\mathbf{y}_{j=0,...,\mathcal{N}}\right\}$ in the inner product space of the Hermitian matrix, which is used in calculating



 $\begin{tabular}{ll} \textbf{Fig. 7.} & \textbf{Estimated angles through EKF and PBLPO with respect to reference in test No. 1.} \end{tabular}$

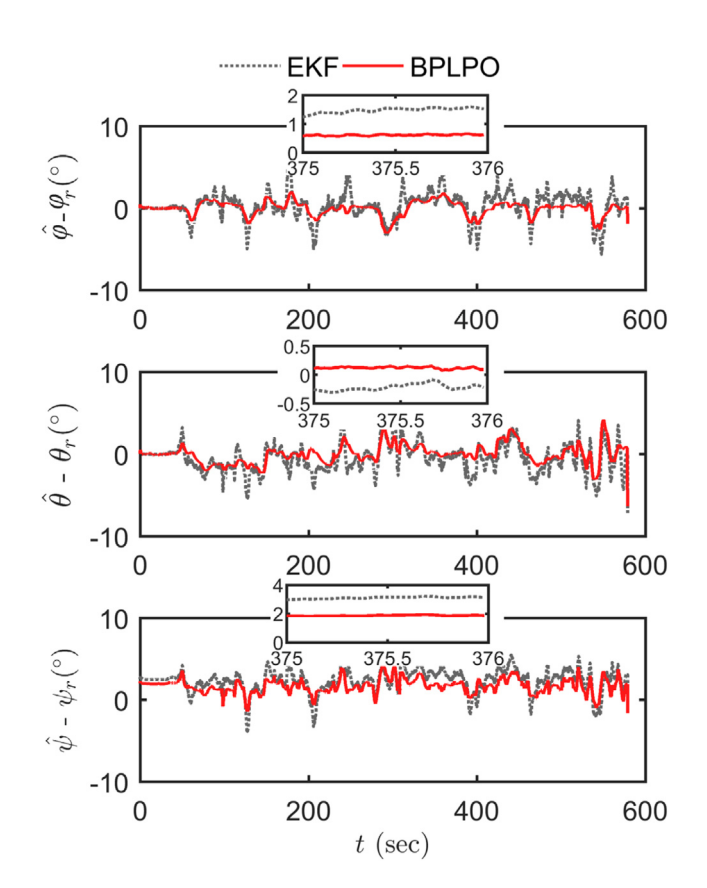
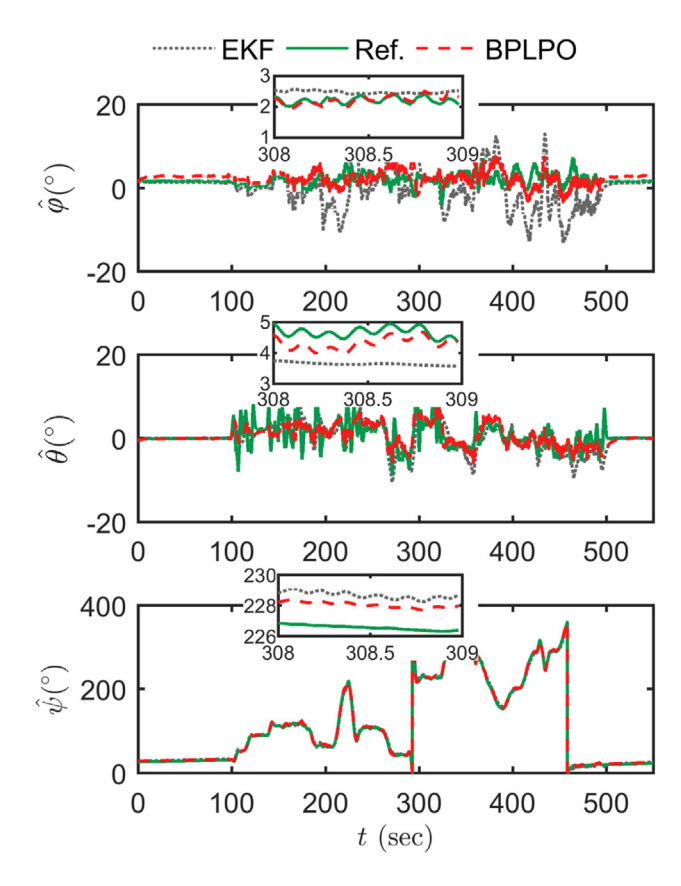
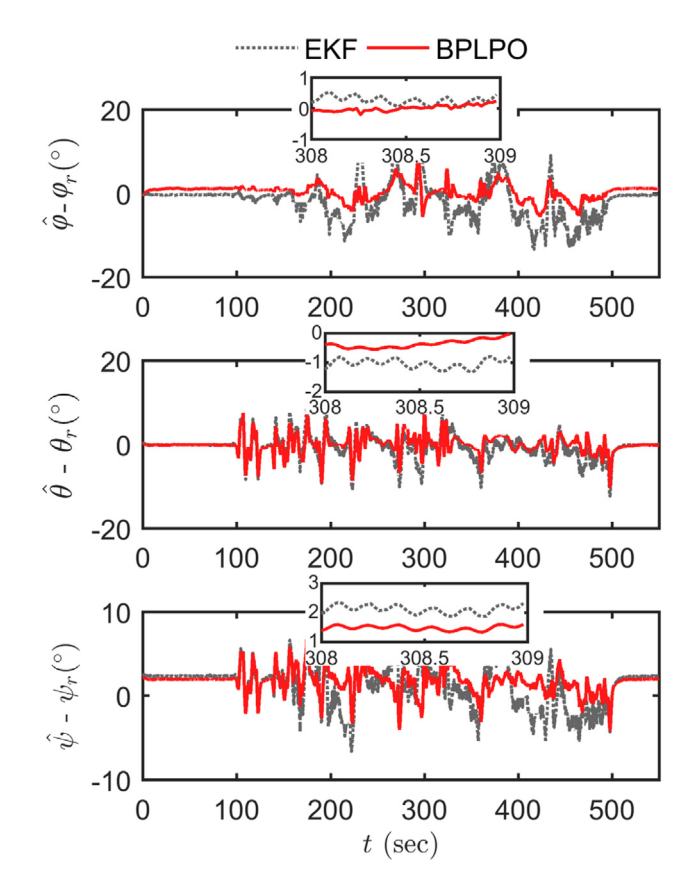


Fig. 8. Estimated angles error through EKF and PBLPO with respect to reference in test No. 1.



 $\pmb{\text{Fig. 9.}}$ Estimated angles through the EKF and PBLPO with respect to reference in test No. 2.



 $\begin{tabular}{ll} \textbf{Fig. 10.} Estimated error angles through the EKF and PBLPO with respect to reference in test No. 2. \end{tabular}$

ISA Transactions xxx (xxxx) xxx

linear independence. Gramian matrix is defined as follows:

$$\mathbf{R}_{zy} = \langle \mathbf{z}, \mathbf{y} \rangle = \begin{bmatrix} \langle \mathbf{z}_0, \mathbf{y}_0 \rangle & \cdots & \langle \mathbf{z}_0, \mathbf{y}_{N} \rangle \\ \vdots & \ddots & \vdots \\ \langle \mathbf{z}_{M}, \mathbf{y}_0 \rangle & \cdots & \langle \mathbf{z}_{M}, \mathbf{y}_{N} \rangle \end{bmatrix}$$
(A.1)

where $\langle \mathbf{z}_i, \mathbf{y}_j \rangle = \mathbf{z}_i \cdot \mathbf{y}_j$. Thus, the set of vectors are linearly independent if and only if the Gramian determinant is non-zero [34].

A.1. Dual basis

Consider the linear set of independent vectors v as:

$$\left\{\mathbf{z}_{i=0,\ldots,\mathcal{M}},\mathbf{y}_{i=0,\ldots,\mathcal{N}}\right\} \tag{A.2}$$

where $\mathbf{y} \triangleq \operatorname{col} \{\mathbf{y}_0, \dots, \mathbf{y}_{\mathcal{N}}\}$ and $\mathbf{z} \triangleq \operatorname{col} \{\mathbf{z}_0, \dots, \mathbf{z}_{\mathcal{M}}\}$. According to the following theory of dual basis, while the amounts of set of vectors $\{\mathbf{y}_i\}$ are available, the quantities of the set of vectors $\{\mathbf{z}_i\}$ can be estimated. The Gramian matrix for this set is shown as follows:

$$\left\langle \begin{bmatrix} \mathbf{z} \\ \mathbf{y} \end{bmatrix}, \begin{bmatrix} \mathbf{z} \\ \mathbf{y} \end{bmatrix} \right\rangle = \begin{bmatrix} \langle \mathbf{z}, \mathbf{z} \rangle & \langle \mathbf{z}, \mathbf{y} \rangle \\ \langle \mathbf{y}, \mathbf{z} \rangle & \langle \mathbf{y}, \mathbf{y} \rangle \end{bmatrix} = \begin{bmatrix} \mathbf{R}_z & \mathbf{R}_{zy} \\ \mathbf{R}_{yz} & \mathbf{R}_y \end{bmatrix}$$
(A.3)

where matrices \mathbf{R}_z and \mathbf{R}_y are nonsingular. For each $a_i, b_i \in S$ the linear space of all vectors produced is represented with $\mathcal{L}\{\mathbf{z}, \mathbf{y}\}$, that:

$$a_0 \mathbf{z}_0 + \dots + a_{\mathcal{M}} \mathbf{z}_{\mathcal{M}} + b_0 \mathbf{y}_0 + \dots + b_{\mathcal{N}} \mathbf{y}_{\mathcal{N}}$$
 (A.4)

The independent linear vectors in Eq. (A.2) illustrate that these vectors are the basis for $\mathcal{L}\{\mathbf{z}, \mathbf{y}\}$. However, the simple form, i.e. $\{\mathbf{z}, \mathbf{y}\}$ is used as the basis for $\mathcal{L}\{\mathbf{z}, \mathbf{y}\}$.

Definition A.2 (*Dual Basis*). For the given basis $\{z, y\}$, the dual basis is shown as $\{z^d, y^d\}$ with two properties as follows [26]:

$$\begin{pmatrix}
\mathbf{z}^{d}, \mathbf{y}^{d} \\
\begin{pmatrix}
\mathbf{z}^{d} \\
\mathbf{y}^{d}
\end{pmatrix}, \begin{bmatrix}
\mathbf{z} \\
\mathbf{y}
\end{bmatrix}
\end{pmatrix} = \begin{bmatrix}
\langle \mathbf{z}^{d}, \mathbf{z} \rangle & \langle \mathbf{z}^{d}, \mathbf{y} \rangle \\
\langle \mathbf{y}^{d}, \mathbf{z} \rangle & \langle \mathbf{y}^{d}, \mathbf{y} \rangle
\end{bmatrix} = \begin{bmatrix}
\mathbf{I} & 0 \\
0 & \mathbf{I}
\end{bmatrix}$$
(A.5)

where \mathbf{y}^d and \mathbf{z}^d are the basis for the same linear space $\mathcal{L}\{\mathbf{z},\mathbf{y}\}$. This basis having properties that include \mathbf{z}^d is orthonormal to \mathbf{y} , as well as \mathbf{y}^d is orthonormal to \mathbf{z} . In addition, \mathbf{z}^d and \mathbf{y}^d are normalized. In other words, $\langle \mathbf{z}^d, \mathbf{z} \rangle = \mathbf{I}$, $\langle \mathbf{y}^d, \mathbf{y} \rangle = \mathbf{I}$ shows the bi-orthogonality condition. However, if $\{\mathbf{z}, \mathbf{y}\}$ is the orthonormal basis; therefore, the dual basis will simply match the main basis.

A.2. Description of algebraic specifications for dual basis

Clearly, $\{z, y\}$ and $\{z^d, y^d\}$ are the span in a linear space, that can be described as follows:

$$\begin{bmatrix} \mathbf{z}^d \\ \mathbf{y}^d \end{bmatrix} = \begin{bmatrix} \mathbf{A}_G & \mathbf{B}_G \\ \mathbf{C}_G & \mathbf{D}_G \end{bmatrix} \begin{bmatrix} \mathbf{z} \\ \mathbf{y} \end{bmatrix}$$
 (A.6)

where $\left[egin{array}{cc} {\pmb A}_G & {\pmb B}_G \\ {\pmb C}_G & {\pmb D}_G \end{array}
ight]$ is a nonsingular block matrix. Therefore:

$$\begin{bmatrix} \mathbf{A}_{G} & \mathbf{B}_{G} \\ \mathbf{C}_{G} & \mathbf{D}_{G} \end{bmatrix} = \begin{bmatrix} \mathbf{R}_{z} & \mathbf{R}_{zy} \\ \mathbf{R}_{yz} & \mathbf{R}_{y} \end{bmatrix}^{-1} \begin{bmatrix} \mathbf{z} \\ \mathbf{y} \end{bmatrix}$$
(A.7)

and the Gramian matrix is:

$$\begin{bmatrix} \mathbf{R}_{z^d} & \mathbf{R}_{z^d y^d} \\ \mathbf{R}_{y^d z^d} & \mathbf{R}_{y^d} \end{bmatrix} = \left\langle \begin{bmatrix} \mathbf{z}^d \\ \mathbf{y}^d \end{bmatrix}, \begin{bmatrix} \mathbf{z}^d \\ \mathbf{y}^d \end{bmatrix} \right\rangle = \begin{bmatrix} \mathbf{R}_z & \mathbf{R}_{zy} \\ \mathbf{R}_{yz} & \mathbf{R}_y \end{bmatrix}^{-1}$$
(A.8)

The results are presented in Eqs. (A.6) to (A.8) may not be intuitive, so the geometric descriptions of the dual basis are given.

A.3. Description of geometric specifications for dual basis

Consider the definitions of $\hat{\mathbf{y}}_{|\mathbf{z}} \triangleq \text{projection of } \mathbf{y} \text{ on } \mathcal{L} \{\mathbf{z}\}$ as well as $\hat{\mathbf{z}}_{|\mathbf{y}} \triangleq \text{projection of } \mathbf{z} \text{ on } \mathcal{L} \{\mathbf{y}\}$. The errors related to these definitions are:

$$\begin{split} \tilde{\mathbf{z}} &\triangleq \tilde{\mathbf{z}}_{|\mathbf{y}} = \mathbf{z} - \hat{\mathbf{z}}_{|\mathbf{y}} \\ \tilde{\mathbf{y}} &\triangleq \tilde{\mathbf{y}}_{|\mathbf{z}} = \mathbf{y} - \hat{\mathbf{y}}_{|\mathbf{z}} \end{split} \tag{A.9}$$

It is emphasized that $\langle \hat{\mathbf{z}}, \mathbf{y} \rangle$ and $\langle \mathbf{z}^d, \mathbf{y} \rangle$ span the same linear space. According to the orthogonal principle of estimation in the least-mean-squares, $\langle \tilde{\mathbf{z}}, \mathbf{y} \rangle = 0$. Combination of these facts with the property $\langle \mathbf{z}^d, \mathbf{y} \rangle = 0$ determine that $\tilde{\mathbf{z}}$ and \mathbf{z}^d must be spanned to the same linear space. Therefore, the nonsingular matrix of \mathbf{M} in the form $\mathbf{z}^d = \mathbf{M}\tilde{\mathbf{z}}$ is required, and the following equations can be concluded:

$$I = \langle \mathbf{z}^{d}, \mathbf{z} \rangle = \mathbf{M} \langle \tilde{\mathbf{z}}, \mathbf{z} \rangle = \mathbf{M} \langle \tilde{\mathbf{z}}, \tilde{\mathbf{z}} + \hat{\mathbf{z}}_{\mathbf{y}} \rangle = \mathbf{M} \langle \tilde{\mathbf{z}}, \tilde{\mathbf{z}} \rangle$$

$$\triangleq \mathbf{M} \mathbf{R}_{\tilde{\mathbf{z}}} \to \mathbf{M} = \mathbf{R}_{\tilde{\mathbf{z}}}^{-1}$$

$$\mathbf{z}^{d} = \mathbf{R}_{\tilde{\mathbf{z}}}^{-1} \tilde{\mathbf{z}}_{|\mathbf{y}|} \quad \text{that} \quad \mathbf{R}_{\tilde{\mathbf{z}}} = \|\tilde{\mathbf{z}}_{|\mathbf{y}|}\|^{2}$$

$$\mathbf{y}^{d} = \mathbf{R}_{\tilde{\mathbf{y}}}^{-1} \tilde{\mathbf{y}}_{|\mathbf{z}} \quad \text{that} \quad \mathbf{R}_{\tilde{\mathbf{y}}} = \|\tilde{\mathbf{y}}_{|\mathbf{z}}\|^{2}$$

$$(A.10)$$

References

- Khankalantary S, Rafatnia S, Mohammadkhani H. An adaptive constrained type-2 fuzzy Hammerstein neural network data fusion scheme for low-cost SINS/GNSS navigation system. Appl Soft Comput 2020;86:105917.
- [2] Farrell JL. Attitude determination by Kalman filtering. Automatica 1970:6(3):419–30.
- [3] Lefferts EL, Markley FL, Shuster M. Kalman filtering for spacecraft attitude estimation. J Guid Control Dyn 1982;5(5):417–29.
- [4] Crassidis JL, Markley FL, Cheng Y. Survey of nonlinear attitude estimation methods. J Guid Control Dyn 2007;30(1):12–28.
- [5] Merhav S, Koifman M. Autonomously aided strapdown attitude reference system. J Guid Control Dyn 1991;14(6):1164–72.
- [6] Crassidis JL, Markley FL. Predictive filtering for attitude estimation without rate sensors. J Guid Control Dyn 1997;20(3):522–7.
- [7] Crassidis JL, Markley FL. Unscented filtering for spacecraft attitude estimation. J Guid Control Dyn 2003;26(4):536–42.
- [8] Zhu R, Sun D, Zhou Z, Wang D. A linear fusion algorithm for attitude determination using low cost MEMS-based sensors. Measurement 2007;40(3):322–8.
- [9] Batista P, Silvestre C, Oliveira P. Globally exponentially stable cascade observers for attitude estimation. Control Eng Pract 2012;20(2):148–55.
- [10] Martin P, Salaün E. An invariant observer for earth-velocity-aided attitude heading reference systems. In: 17th world congress the international federation of automatic control, Seoul, Korea; 2008. p. 9857–64.
- [11] Sabatini AM. Quaternion-based extended Kalman filter for determining orientation by inertial and magnetic sensing. IEEE Trans Biomed Eng 2006;53(7):1346–56.
- [12] Lee JK, Park EJ, Robinovitch SN. Estimation of attitude and external acceleration using inertial sensor measurement during various dynamic conditions. IEEE Trans Instrum Meas 2012;61(8):2262–73.
- [13] Martin P, Salaün E. Design and implementation of a low-cost observer-based attitude and heading reference system. Control Eng Pract 2010;18(7):712–22.
- [14] Ali SD, Bhatti UI, Munawwar K, Al-Saggaf U, Mansoor S, Ali J. Gyroscopic drift compensation by using low cost sensors for improved attitude determination. Measurement 2018;116:199–206.
- [15] Markley L. Attitude determination using two vector measurements. In: Flight mechanics symposium. Greenbelt, MD: NASA Goddard Space Flight Center; 1999, p. 39–52.
- [16] Rehbinder H, Hu X. Drift-free attitude estimation for accelerated rigid bodies. Automatica 2004;40(4):653–9.
- [17] Tang X, Liu Z, Zhang J. Square-root quaternion cubature Kalman filtering for spacecraft attitude estimation. Acta Astronaut 2012;76:84–94.
- [18] Huang W, Xie H, Shen C, Li J. A robust strong tracking cubature Kalman filter for spacecraft attitude estimation with quaternion constraint. Acta Astronaut 2016;121:153–63.
- [19] de Celis R, Cadarso L. Attitude determination algorithms through accelerometers, GNSS sensors, and gravity vector estimator. Int J Aerosp Eng 2018;2018(2). 5394057.
- [20] Soken HE, Hajiyev C. Pico satellite attitude estimation via robust unscented Kalman filter in the presence of measurement faults. ISA Trans 2010;49(3):249–56.

ARTICLE IN PRESS

J. Keighobadi, J. Faraji, F. Janabi-Sharifi et al.

ISA Transactions xxx (xxxx) xxx

- [21] Bolandi H, Fani Saberi F, Mehrjardi Eslami A. Design of an extended interacting multiple models adaptive estimator for attitude determination of a stereoimagery satellite. Int J Aerosp Eng 2011;2011:1–19.
- [22] No H, Cho A, Kee C. Attitude estimation method for small UAV under accelerative environment. GPS Solut 2015;19(3):343–55.
- [23] Zhang D, Nie G. Adaptive attitude quaternion Kalman filter based on factored quaternions. Control Theory Appl 2018;35(3):367–74.
- [24] Yang Y. An intelligent quaternion SVDCKF AHRS estimation with variable adaptive methods in complex conditions. 2020, arXiv preprint arXiv:2002. 03920
- [25] Keighobadi J, Hosseini-Pishrobat M, Faraji J, Naseri Langehbiz M. Design and experimental evaluation of immersion and invariance observer for low-cost attitude-heading reference system. IEEE Trans Ind Electron 2019:67(9):7871–8.
- [26] Keighobadi J, Vosoughi H, Faraji J. Design and implementation of a model predictive observer for AHRS. GPS Solut 2018;22(1):29.
- [27] Maleknejad K, Basirat B, Hashemizadeh E. Hybrid Legendre polynomials and Block-Pulse functions approach for nonlinear Volterra-Fredholm integro-differential equations. Comput Math Appl 2011;61(9):2821-8.
- [28] Mohan B, Kar SK. Optimal control of nonlinear systems via block pulse functions and Legendre polynomials. Differ Equ Dyn Syst 2012;20(2):149–59.
- [29] Shahrezaee M. Solving an integro-differential equation by Legendre polynomial and block-pulse functions. In: Dynamical systems and applications, Antalya, Turkey; 2004. p. 642–7.

- [30] Mashayekhi S, Razzaghi M, Wattanataweekul M. Analysis of multi-delay and piecewise constant delay systems by hybrid functions approximation. Differ Equ Dyn Syst 2016;24(1):1–20.
- [31] Rafatnia S, Nourmohammadi H, Keighobadi J, Badamchizadeh M. Inmove aligned SINS/GNSS system using recurrent wavelet neural network (RWNN)-based integration scheme. Mechatronics 2018;54:155–65.
- [32] Rafatnia S, Nourmohammadi H, Keighobadi J. Fuzzy-adaptive constrained data fusion algorithm for indirect centralized integrated SINS/GNSS navigation system. GPS Solut 2019;23(3):62.
- [33] Titterton D, Weston JL, Weston J. Strapdown inertial navigation technology. London: The Institution of Engineering and Technology; 2004.
- [34] Kailath T, Sayed AH, Hassibi B. Linear estimation. Prentice Hall; 2000.
- [35] Marzban HR, Pirmoradian H. A direct approach for the solution of nonlinear optimal control problems with multiple delays subject to mixed state-control constraints. Appl Math Model 2018;53:189–213.
- [36] Razzaghi M, Marzban H-R. A hybrid analysis direct method in the calculus of variations. Int J Comput Math 2000;75(3):259–69.
- [37] Marzban H, Razzaghi M. Hybrid functions approach for linearly constrained quadratic optimal control problems. Appl Math Model 2003;27(6):471–85.
- [38] Lancaster P, Tismenetsky M. The theory of matrices: with applications. 2nd ed. Orlando: Academic Press; 1985.
- [39] Dorf RC, Bishop RH. Modern control systems, (Pearson, 2011).